

# Numerical analysis of superconducting phases in the extended Hubbard model with non-local pairing

University of Pisa, a.y. 2025-2026

Alessandro Gori\*

Thesis for the Master's degree in Physics

## Abstract

[To be continued...]

## Contents

<b>1</b>	<b>Theoretical introduction</b>	<b>3</b>
1.1	Antiferromagnetic ordering in the Hubbard model	3
1.2	The Extended Fermi-Hubbard model	3
1.2.1	Experimental insight on NN attraction	4
<b>2</b>	<b>Mean-field theory analysis of the EHM</b>	<b>5</b>
2.1	Mean-Field theory real space description	5
2.1.1	The non-local term as a source of symmetry-breaking interactions	6
2.1.2	Reciprocal-space transform of the non-local interaction	8
2.2	Anti-Ferromagnetic instability	9
2.2.1	Hartree renormalization of chemical potential and gap	10
2.2.2	Fock renormalization of the hopping amplitude	12
2.2.3	Renormalized hamiltonian behavior	16
2.2.4	Results of the HF algorithm	16
2.3	Superconducting instability	16
2.3.1	Mean-field treatment of the non-local term	17
2.3.2	Mean-field treatment of the local term	17
2.3.3	Topological correlations	18
2.4	Mean-Field theory reciprocal space description	19
2.4.1	Kinetic term	19
2.4.2	Non-local attraction	19
2.4.3	Local interaction and gap function	21
2.4.4	Nambu formalism and Bogoliubov transform	22
2.4.5	A short comment on self-consistency	24
2.5	Results of the HF algorithm	24
<b>3</b>	<b>Superexchange and virtual hopping in Hubbard lattices</b>	<b>25</b>
3.1	Virtual hopping in the 2-sites Hubbard lattice	25
3.1.1	Exact solution of the half-filled model	26
3.1.2	Virtual hopping	26

---

\*a.gori23@studenti.unipi.it / nepero27178@github.com

<b>4</b>	<b>Mean-Field Theory in Hubbard lattices</b>	<b>27</b>
4.1	Ferromagnetic solution . . . . .	27
4.2	Antiferromagnetic solution . . . . .	28
4.2.1	Theoretical mean-field solution . . . . .	32
4.2.2	Hartree-Fock algorithm in reciprocal space . . . . .	33
4.2.3	An alternative (less efficient) real-space approach . . . . .	35
	<b>Bibliography</b>	<b>39</b>

#### **List of symbols and abbreviations**

---

AF	Anti-Ferromagnetic
BCS	Bardeen-Cooper-Schrieffer (theory)
DoF	Degree of Freedom
HF	Hartree-Fock
MFT	Mean-Field Theory
SC	Superconductor
$T_c$	Critical temperature



# Introduction

This thesis project is about my favorite ice cream flavor. [To be continued...]



# Chapter 1

## Theoretical introduction

[To be continued...]

### 1.1 Antiferromagnetic ordering in the Hubbard model

Consider the ordinary Hubbard model:

$$\hat{H} = -t \sum_{\langle ij \rangle} \sum_{\sigma} \hat{c}_{i\sigma}^{\dagger} \hat{c}_{j\sigma} + U \sum_i \hat{n}_{i\uparrow} \hat{n}_{i\downarrow} \quad t, U > 0 \quad (1.1)$$

The two competing mechanisms are site-hopping of amplitude  $t$  and local repulsion of amplitude  $U$ . For this model defined **on a bipartite lattice at half filling** and fixed electron number, it is well known [6] that, below a certain critical temperature  $T_c$  and above some (small) critical repulsion  $U_c/t$ , the ground-state acquires antiferromagnetic (AF) long-range ordering, schematically depicted in Fig. 1.1a. The mechanism for the formation of the AF phase takes advantage of virtual hopping, as described in App. 3; the Mean-Field Theory (MFT) treatment of ferromagnetic-antiferromagnetic orderings in 2D Hubbard lattices is discussed in App. 4.

In this chapter the discussion is limited to the two-dimensional square lattice Hubbard model. The lattice considered has  $L_{\ell}$  sites on side  $\ell = x, y$ , thus a total of  $L_x L_y$  sites. The total number of single electron states is given by  $D = 2L_x L_y$ . All theoretical discussion neglects border effects, thus considering  $D \rightarrow +\infty$ .

### 1.2 The Extended Fermi-Hubbard model

The Extended Fermi-Hubbard model is defined by:

$$\hat{H} = -t \sum_{\langle ij \rangle} \sum_{\sigma} \hat{c}_{i\sigma}^{\dagger} \hat{c}_{j\sigma} + U \sum_i \hat{n}_{i\uparrow} \hat{n}_{i\downarrow} - V \sum_{\langle ij \rangle} \sum_{\sigma \sigma'} \hat{n}_{i\sigma} \hat{n}_{j\sigma'} \quad (1.2)$$

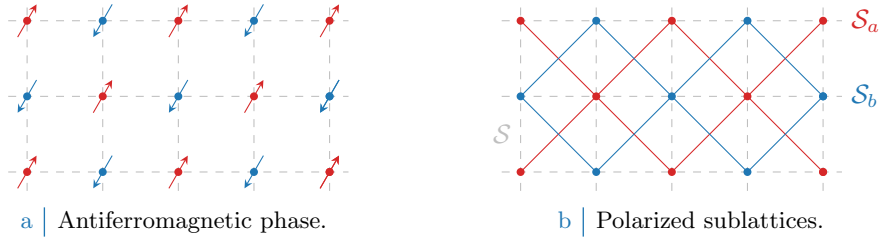


**Figure 1.1** | Schematic representation of the AF phase. Fig. 1.1a shows a portion of the square lattice with explicit representation of the spin for each site. Fig. 1.1b divides the square lattice  $\mathcal{S}$  in two polarized sublattices  $\mathcal{S}_a, \mathcal{S}_b$ . The AF phase results from the interaction of two inversely polarized “ferromagnetic” square lattices.

Note that, on a square lattice, we can perform the summation over NN just as

$$\sum_{\langle ij \rangle} \equiv \sum_{i \in \mathcal{S}_a} [\delta_{j=i+\delta_x} + \delta_{j=i-\delta_x} + \delta_{j=i+\delta_y} + \delta_{j=i-\delta_y}]$$

where notation of Fig. 1.1b has been used. The last term represents an effective attraction between neighboring electrons, of amplitude  $V$ . Such an interaction is believed [1] necessary to describe the insurgence of high- $T_c$  superconductivity in cuprate SCs. [To be continued...]

### 1.2.1 Experimental insight on NN attraction

Todo:

- High  $T_c$  SC in cuprates;
- Experimental evidence of topological SC;
- Insertion of the non-local attraction;



## Chapter 2

# Mean-field theory analysis of the EHM

This chapter is devoted to develop a Mean Field Theory (MFT) approximation of the Extended Hubbard model (EHM) of Eq. (1.2),

$$\hat{H} = \underbrace{-t \sum_{\langle ij \rangle} \sum_{\sigma} \hat{c}_{i\sigma}^{\dagger} \hat{c}_{j\sigma}}_{\hat{H}_t} + \underbrace{U \sum_i \hat{n}_{i\uparrow} \hat{n}_{i\downarrow}}_{\hat{H}_U} - \underbrace{V \sum_{\langle ij \rangle} \sum_{\sigma\sigma'} \hat{n}_{i\sigma} \hat{n}_{j\sigma'}}_{\hat{H}_V}$$

Mean Field Theory (MFT) is a widely used and simple theoretical tool, often sufficient to describe the leading orders in phase transition phenomena of Many-Body Physics. Here MFT is employed to discuss both the effects of the non-local term  $\hat{H}_V$  onto the AF phase, as well as the insurgence of anisotropic superconductivity – following the path of Bardeen-Cooper-Schrieffer (BCS) theory in describing conventional *s*-wave superconductivity. As will be thoroughly described, the lattice spatial structure directly influences the topology of the gap function, giving rise to anisotropic pairing. Sec. 2.1 studies the non-local attraction  $\hat{H}_V$  in real-space, describing how such interaction can contribute to the hamiltonian as a symmetry-breaking term in given channels. In the following sections, we move to specific channels and study theoretically and numerically the effect of non-local attraction.

### 2.1 Mean-Field theory real space description

The general aim is to study the phase diagram of the model by comparing ground-state energies of different phases. The phases we consider here for the EHM are the Anti-Ferromagnetic ordering (AF), given by a non-uniform distribution of charge in each spin sector, and the Superconducting phase, described by a uniformly distributed charge allowing for Cooper pairing instabilities. For the EHM, three symmetries are “brekable”:

1. (Crystal) translational invariance. By breaking explicitly this symmetry, the obtained state must show a Charge-Density Wave (CDW) ordering;
2. U(1) charge conservation. By breaking this symmetry, we allow for Cooper fluctuations originating superconductivity;
3. SU(2) spin conservation. By breaking this symmetry, we take in all the processes not conserving spin (such as site hop *plus* spin flip).

As a general rule, SU(2) symmetry will be preserved while charge and space symmetries will be alternatively broken, in order to generate a pure AF phase or a pure superconducting phase. “To preserve one symmetry” means to set to zero all operators which break said symmetry, due to selection rules.

App. 4 describes in detail the MFT treatment of the pure Hubbard model,  $\hat{H}_t + \hat{H}_U$ ; the key passage is there given by the approximation

$$\hat{n}_{i\uparrow} \hat{n}_{i\downarrow} \simeq \hat{n}_{i\uparrow} \langle \hat{n}_{i\downarrow} \rangle + \langle \hat{n}_{i\uparrow} \rangle \hat{n}_{i\downarrow} + (\text{constants}) \quad (2.1)$$

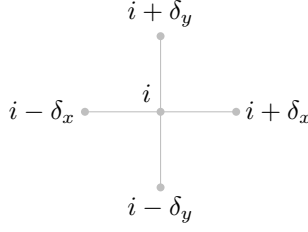


Figure 2.1 | Schematic representation of the four NNs of a given site  $i$  for a planar square lattice.

from which the AF structure is simply recovered. However, to perform the above approximation coherently, we are implementing Wick's Theorem on the generic term:

$$\langle \hat{c}_{i\sigma}^\dagger \hat{c}_{j\sigma'}^\dagger \hat{c}_{j\sigma'} \hat{c}_{i\sigma} \rangle \simeq \underbrace{\langle \hat{c}_{i\sigma}^\dagger \hat{c}_{j\sigma'}^\dagger \rangle \langle \hat{c}_{j\sigma'} \hat{c}_{i\sigma} \rangle}_{\text{Cooper}} - \underbrace{\langle \hat{c}_{i\sigma}^\dagger \hat{c}_{j\sigma'} \rangle \langle \hat{c}_{j\sigma'}^\dagger \hat{c}_{i\sigma} \rangle}_{\text{Fock}} + \underbrace{\langle \hat{c}_{i\sigma}^\dagger \hat{c}_{i\sigma} \rangle \langle \hat{c}_{j\sigma'}^\dagger \hat{c}_{j\sigma'} \rangle}_{\text{Hartree}} \quad (2.2)$$

As a first approximation, the theorem is assumed to hold (which, in a BCS-like fashion, is equivalent to assuming for the ground-state to be a coherent state). Of the three terms above, the AF phase description for the pure Hubbard Model only allows for the Hartree term to be non-zero. Cooper fluctuations are suppressed, because only the translational invariance is broken, and the Fock term is null as well because if  $i = j$  and  $\sigma' = \bar{\sigma}$  (as is for the local interaction, which contains the operator  $\hat{n}_{i\uparrow} \hat{n}_{i\downarrow}$ ) the expectation values involved are describing a process breaking SU(2) spin symmetry. Thus, correctly, the Wick's decomposition of Eq. (2.1) only involves Hartree-terms of Eq. (2.2). In general, however, the three terms need to be considered altogether: this is what is done in the next section.

[ Insert here a comment anticipating the discussion of different symmetry structures ( $s, s^*, p_x, p_y, d_{x^2-y^2}$ ). ]

### 2.1.1 The non-local term as a source of symmetry-breaking interactions

Consider now the NN non-local term,

$$\hat{H}_V \equiv -V \sum_{\langle ij \rangle} \sum_{\sigma\sigma'} \hat{n}_{i\sigma} \hat{n}_{j\sigma'} \quad (2.3)$$

Evidently the hamiltonian can be decomposed in various spin terms,

$$\begin{aligned} \hat{H}_V &= \sum_{\sigma\sigma'} \hat{H}_V^{\sigma\sigma'} \\ &= \underbrace{\hat{H}_V^{\uparrow\uparrow} + \hat{H}_V^{\downarrow\downarrow}}_{\text{Same-spin}} + \underbrace{\hat{H}_V^{\uparrow\downarrow} + \hat{H}_V^{\downarrow\uparrow}}_{\text{Opposite-spin}} \end{aligned}$$

Evidently, to carry out a summation over nearest neighbors  $\langle ij \rangle$  of a square lattice means precisely to sum over all links of the lattice. Then we can identify the generic opposite-spin (o.s.) term  $\hat{H}_V^{\sigma\bar{\sigma}}$  as the one collecting the  $\sigma$  operators of sublattice  $\mathcal{S}_a$  and  $\bar{\sigma}$  operators of sublattice  $\mathcal{S}_b$ . The o.s. non-local interactions can be written as a sum of terms over just one of the two sublattices  $\mathcal{S}_a$  and  $\mathcal{S}_b$ , oppositely polarized in the AF configuration (see Fig. 1.1b)

$$\begin{aligned} \hat{H}_V^{(\text{o.s.})} &= \sum_{i \in \mathcal{S}_a} \hat{h}_V^{(i)} + \sum_{i \in \mathcal{S}_b} \hat{h}_V^{(i)} \\ &= \sum_{i \in \mathcal{S}} \hat{h}_V^{(i)} \end{aligned} \quad \hat{h}_V^{(i)} = -V \sum_{\ell=x,y} (\hat{n}_{i\uparrow} \hat{n}_{i+\delta_\ell\downarrow} + \hat{n}_{i\uparrow} \hat{n}_{i-\delta_\ell\downarrow})$$

Here the notation of Fig. 1.1b is used. The two-dimensional lattice is regular-square. For each site  $i$  in a given sublattice, the nearest neighbors sites are four – all in the other sublattice. The

notation used is  $i \pm \delta_x$ ,  $i \pm \delta_y$  as in Fig. 2.1. Similarly, the same-spin (s.s.) hamiltonian decomposes as

$$\hat{H}_V^{(\text{s.s.})} = -V \sum_{i \in S_a} \sum_{\ell=x,y} \sum_{\sigma} (\hat{n}_{i\sigma} \hat{n}_{i+\delta_\ell\sigma} + \hat{n}_{i\sigma} \hat{n}_{i-\delta_\ell\sigma})$$

Note here the summation only on one sublattice. The non-local interaction contribution to energy, as a function of the  $T = 0$  full hamiltonian ground-state<sup>1</sup>  $|\Psi\rangle$ , is given by

$$\begin{aligned} E_V[\Psi] &= \langle \Psi | \hat{H}_V | \Psi \rangle \\ &= -V \sum_{\langle ij \rangle} \sum_{\sigma\sigma'} \langle \hat{n}_{i\sigma} \hat{n}_{j\sigma'} \rangle \\ &= -V \underbrace{\sum_{\langle ij \rangle} \sum_{\sigma} \langle \hat{n}_{i\sigma} \hat{n}_{j\sigma} \rangle}_{\text{s.s.}} - V \underbrace{\sum_{\langle ij \rangle} \sum_{\sigma} \langle \hat{n}_{i\sigma} \hat{n}_{j\bar{\sigma}} \rangle}_{\text{o.s.}} \end{aligned}$$

Shorthand notation has been used:  $\langle \Psi | \cdot | \Psi \rangle = \langle \cdot \rangle$ . The ground-state must realize the condition

$$\frac{\delta}{\delta \langle \Psi |} E[\Psi] = 0$$

being  $E[\Psi]$  the total energy (made up of the three terms of couplings  $t$ ,  $U$  and  $V$ ). [\[Expand derivation?\]](#) The functional derivative must be carried out in a variational fashion including a Lagrange multiplier, the latter accounting for state-norm conservation, as is done normally in deriving the Hartree-Fock approximation for the eigenenergies of the electron liquid [4, 5].

**Opposite-spin terms.** Consider first the o.s. terms: take e.g. the term  $\hat{n}_{i\uparrow} \hat{n}_{i+\delta_x\downarrow}$ . As in Eq. (2.2), Wick's Theorem states that, if the expectation value is performed onto a coherent state,

$$\begin{aligned} \langle \hat{n}_{i\uparrow} \hat{n}_{i+\delta_x\downarrow} \rangle &= \langle \hat{c}_{i\uparrow}^\dagger \hat{c}_{i+\delta_x\downarrow}^\dagger \hat{c}_{i+\delta_x\downarrow} \hat{c}_{i\uparrow} \rangle \\ &= \underbrace{\langle \hat{c}_{i\uparrow}^\dagger \hat{c}_{i+\delta_x\downarrow}^\dagger \rangle \langle \hat{c}_{i+\delta_x\downarrow} \hat{c}_{i\uparrow} \rangle}_{\text{Cooper}} - \underbrace{\langle \hat{c}_{i\uparrow}^\dagger \hat{c}_{i+\delta_x\downarrow} \rangle \langle \hat{c}_{i+\delta_x\downarrow}^\dagger \hat{c}_{i\uparrow} \rangle}_{\text{Fock}} + \underbrace{\langle \hat{c}_{i\uparrow}^\dagger \hat{c}_{i\uparrow} \rangle \langle \hat{c}_{i+\delta_x\downarrow}^\dagger \hat{c}_{i+\delta_x\downarrow} \rangle}_{\text{Hartree}} \end{aligned}$$

Identical decompositions are given for all others NNs. Of the three terms above:

- The Cooper term breaks U(1) charge symmetry, allowing for superconducting instabilities;
- The Fock term breaks the SU(2) symmetry, because it accounts for a site hop *plus* spin flip process;
- The Hartree term breaks translational invariance, because the mean-field to interact with is given by the local density;

Then, to look for AF instability only the Hartree term is to be accounted; instead, in superconducting instability only the Cooper term contributes. The Fock term we always assume to be suppressed, preserving SU(2) symmetry. Note that for superconducting instabilities, due to superexchange mechanism (as explained in App. 4) the o.s. term account for singlet pairing as well as zero-spin triplet pairing. Which channel is preferred, is a matter of thermodynamic advantage.

**Same-spin terms.** Consider then the same-spin terms: take e.g. the term  $\hat{n}_{i\uparrow} \hat{n}_{i+\delta_x\uparrow}$ . As above,

$$\begin{aligned} \langle \hat{n}_{i\uparrow} \hat{n}_{i+\delta_x\uparrow} \rangle &= \langle \hat{c}_{i\uparrow}^\dagger \hat{c}_{i+\delta_x\uparrow}^\dagger \hat{c}_{i+\delta_x\uparrow} \hat{c}_{i\uparrow} \rangle \\ &= \underbrace{\langle \hat{c}_{i\uparrow}^\dagger \hat{c}_{i+\delta_x\uparrow}^\dagger \rangle \langle \hat{c}_{i+\delta_x\uparrow} \hat{c}_{i\uparrow} \rangle}_{\text{Cooper}} - \underbrace{\langle \hat{c}_{i\uparrow}^\dagger \hat{c}_{i+\delta_x\uparrow} \rangle \langle \hat{c}_{i+\delta_x\uparrow}^\dagger \hat{c}_{i\uparrow} \rangle}_{\text{Fock}} + \underbrace{\langle \hat{c}_{i\uparrow}^\dagger \hat{c}_{i\uparrow} \rangle \langle \hat{c}_{i+\delta_x\uparrow}^\dagger \hat{c}_{i+\delta_x\uparrow} \rangle}_{\text{Hartree}} \end{aligned}$$

<sup>1</sup>Extensions to finite temperatures is simple: minimization must be carried out on free energy, while expectation values must be taken in a thermodynamic fashion.

Identical consideration as in the above paragraph hold for each term. The only difference with the o.s. terms is given by the Fock term: since the spin-flip process is absent, now the Fock fluctuations actually contribute to the AF phase as an effective NN hopping term [Unclear: does the renormalization happen also for the Cooper phase?]. As a final remark, notice that the superconducting instabilities of the s.s. terms account only for triplet pairing. The only possible superconducting ordering established by the means of these terms is odd in real space. Then  $s$ -wave and  $d$ -wave superconductivity cannot establish in this channel;  $p_\ell$ -wave superconductivity, instead, can.

### 2.1.2 Reciprocal-space transform of the non-local interaction

It is useful to derive analytically the reciprocal-space form of the non-local attraction. Consider a generic bond, say, the one connecting sites  $j$  and  $j \pm \delta_\ell$  (variable  $i$  is here referred to as the imaginary unit to avoid confusion).  $\mathbf{x}_j$  is the 2D notation for the position of site  $j$ , while  $\delta_\ell$  is the 2D notation for the lattice spacing previously indicated as  $\delta_\ell$ . Fourier transform it according to the convention

$$\hat{c}_{j\sigma} = \frac{1}{\sqrt{L_x L_y}} \sum_{\mathbf{k} \in \text{BZ}} e^{-i\mathbf{k} \cdot \mathbf{x}_j} \hat{c}_{\mathbf{k}\sigma}$$

Then:

$$\begin{aligned} \hat{n}_{j\sigma} \hat{n}_{j \pm \delta_\ell \sigma'} &= \hat{c}_{j\sigma}^\dagger \hat{c}_{j \pm \delta_\ell \sigma'}^\dagger \hat{c}_{j \pm \delta_\ell \sigma'} \hat{c}_{j\sigma} \\ &= \frac{1}{(L_x L_y)^2} \sum_{\nu=1}^4 \sum_{\mathbf{k}_\nu \in \text{BZ}} e^{i[(\mathbf{k}_1 + \mathbf{k}_2) - (\mathbf{k}_3 + \mathbf{k}_4)] \cdot \mathbf{x}_j} e^{\pm i(\mathbf{k}_2 - \mathbf{k}_3) \cdot \delta_\ell} \hat{c}_{\mathbf{k}_1 \sigma}^\dagger \hat{c}_{\mathbf{k}_2 \sigma'}^\dagger \hat{c}_{\mathbf{k}_3 \sigma'} \hat{c}_{\mathbf{k}_4 \sigma} \end{aligned}$$

Then, the interaction at site  $j$ , spin  $\sigma$  with its NNs at spin  $\sigma'$  – indicated as  $(j\sigma\sigma')$  – is given by

$$\begin{aligned} (j\sigma\sigma') &= -V \sum_{\ell=x,y} \sum_{\delta=\pm\delta_\ell} \hat{n}_{j\sigma} \hat{n}_{j \pm \delta_\ell \sigma'} \\ &= -\frac{V}{(L_x L_y)^2} \sum_{\ell=x,y} \sum_{\nu=1}^4 \sum_{\mathbf{k}_\nu \in \text{BZ}} e^{i[(\mathbf{k}_1 + \mathbf{k}_2) - (\mathbf{k}_3 + \mathbf{k}_4)] \cdot \mathbf{x}_j} \\ &\quad \times \left( e^{i(\mathbf{k}_2 - \mathbf{k}_3) \cdot \delta_\ell} + e^{-i(\mathbf{k}_2 - \mathbf{k}_3) \cdot \delta_\ell} \right) \hat{c}_{\mathbf{k}_1 \sigma}^\dagger \hat{c}_{\mathbf{k}_2 \sigma'}^\dagger \hat{c}_{\mathbf{k}_3 \sigma'} \hat{c}_{\mathbf{k}_4 \sigma} \\ &= -\frac{2V}{(L_x L_y)^2} \sum_{\ell=x,y} \sum_{\nu=1}^4 \sum_{\mathbf{k}_\nu \in \text{BZ}} e^{i[(\mathbf{k}_1 + \mathbf{k}_2) - (\mathbf{k}_3 + \mathbf{k}_4)] \cdot \mathbf{x}_j} \cos[(\mathbf{k}_2 - \mathbf{k}_3) \cdot \delta_\ell] \hat{c}_{\mathbf{k}_1 \sigma}^\dagger \hat{c}_{\mathbf{k}_2 \sigma'}^\dagger \hat{c}_{\mathbf{k}_3 \sigma'} \hat{c}_{\mathbf{k}_4 \sigma} \end{aligned}$$

The full non-local interaction is given by summing over all sites of  $\mathcal{S}_a$  (which is, half the sites of  $\mathcal{S}$ ). This gives back momentum conservation,

$$\frac{1}{L_x L_y} \sum_{j \in \mathcal{S}_a} e^{i[(\mathbf{k}_1 + \mathbf{k}_2) - (\mathbf{k}_3 + \mathbf{k}_4)] \cdot \mathbf{x}_j} = \frac{1}{2} \delta_{\mathbf{k}_1 + \mathbf{k}_2 = \mathbf{k}_3 + \mathbf{k}_4}$$

Let  $\mathbf{k}_1 + \mathbf{k}_2 = \mathbf{k}_3 + \mathbf{k}_4 = \mathbf{K}$ , and define  $\mathbf{k}, \mathbf{k}'$  such that

$$\mathbf{k}_1 \equiv \mathbf{K} + \mathbf{k} \quad \mathbf{k}_2 \equiv \mathbf{K} - \mathbf{k} \quad \mathbf{k}_3 \equiv \mathbf{K} - \mathbf{k}' \quad \mathbf{k}_4 \equiv \mathbf{K} + \mathbf{k}' \quad \delta \mathbf{k} \equiv \mathbf{k} - \mathbf{k}'$$

Sums over these variables must be intended as over the Brillouin Zone (BZ). Then, finally

$$\begin{aligned} \hat{H}_V &= \sum_{j \in \mathcal{S}_a} \sum_{\sigma\sigma'} (j\sigma\sigma') \\ &= -\frac{V}{L_x L_y} \sum_{\ell=x,y} \sum_{\mathbf{K}, \mathbf{k}, \mathbf{k}'} \cos(\delta \mathbf{k} \cdot \delta_\ell) \hat{c}_{\mathbf{K} + \mathbf{k}\sigma}^\dagger \hat{c}_{\mathbf{K} - \mathbf{k}\sigma'}^\dagger \hat{c}_{\mathbf{K} - \mathbf{k}'\sigma'} \hat{c}_{\mathbf{K} + \mathbf{k}'\sigma} \\ &= -\frac{V}{L_x L_y} \sum_{\mathbf{K}, \mathbf{k}, \mathbf{k}'} [\cos(\delta k_x) + \cos(\delta k_y)] \hat{c}_{\mathbf{K} + \mathbf{k}\sigma}^\dagger \hat{c}_{\mathbf{K} - \mathbf{k}\sigma'}^\dagger \hat{c}_{\mathbf{K} - \mathbf{k}'\sigma'} \hat{c}_{\mathbf{K} + \mathbf{k}'\sigma} \end{aligned} \quad (2.4)$$

Different Wick contraction schemes lead to different results:

$$\overbrace{c_{\mathbf{K}+\mathbf{k}\sigma}^\dagger c_{\mathbf{K}-\mathbf{k}\sigma'}^\dagger c_{\mathbf{K}-\mathbf{k}'\sigma'} c_{\mathbf{K}+\mathbf{k}'\sigma}}^{\text{Cooper contraction}} \quad (2.5)$$

$$\overbrace{c_{\mathbf{K}+\mathbf{k}\sigma}^\dagger c_{\mathbf{K}-\mathbf{k}\sigma'}^\dagger c_{\mathbf{K}-\mathbf{k}'\sigma'} c_{\mathbf{K}+\mathbf{k}'\sigma}}^{\text{Fock contraction}} \quad (2.6)$$

$$\overbrace{c_{\mathbf{K}+\mathbf{k}\sigma}^\dagger c_{\mathbf{K}-\mathbf{k}\sigma'}^\dagger c_{\mathbf{K}-\mathbf{k}'\sigma'} c_{\mathbf{K}+\mathbf{k}'\sigma}}^{\text{Hartree contraction}} \quad (2.7)$$

[To be continued...]

## 2.2 Anti-Ferromagnetic instability

In this section, the effect of the non-local interaction on the antiferromagnetic phase is discussed. The MFT derivation for the “standard” Hubbard Model is discussed in App. 4. Recalling the main results, the Anti-Ferromagnetic phase specified by the Ansatz (4.1) (which is explicitly breaking translational invariance in each spin sector, while preserving SU(2) and U(1) symmetries) reduces the hamiltonian to the form of Eq. (4.2)

$$\hat{H}_t + \hat{H}_U \stackrel{\text{MFT}}{\simeq} -t \sum_{\langle \mathbf{r}\mathbf{r}' \rangle} \sum_{\sigma} \hat{c}_{\mathbf{r}\sigma}^\dagger \hat{c}_{\mathbf{r}'\sigma} + nU \sum_{\mathbf{r}} [\hat{n}_{\mathbf{r}\uparrow} + \hat{n}_{\mathbf{r}\downarrow}] - mU \sum_{\mathbf{r}} (-1)^{x+y} [\hat{n}_{\mathbf{r}\uparrow} - \hat{n}_{\mathbf{r}\downarrow}]$$

In reciprocal space, the hamiltonian decomposes as in Eq. (4.4),

$$\hat{H}_t + \hat{H}_U \stackrel{\text{MFT}}{\simeq} \sum_{\mathbf{k} \in \text{MBZ}} \sum_{\sigma} \hat{\Psi}_{\mathbf{k}\sigma}^\dagger h_{\mathbf{k}\sigma} \hat{\Psi}_{\mathbf{k}\sigma} \quad \text{being} \quad h_{\mathbf{k}\sigma} \equiv \begin{bmatrix} \epsilon_{\mathbf{k}} & -\Delta_{\sigma} \\ -\Delta_{\sigma} & -\epsilon_{\mathbf{k}} \end{bmatrix}$$

and  $\Delta_{\uparrow} = mU$ ,  $\Delta_{\downarrow} = -mU$ . Nambu spinorial formulation is used,

$$\hat{\Psi}_{\mathbf{k}\sigma} \equiv \begin{bmatrix} \hat{c}_{\mathbf{k}\sigma} \\ \hat{c}_{\mathbf{k}+\pi\sigma} \end{bmatrix}$$

and the free electrons energy is simply the tight binding energy

$$\epsilon_{\mathbf{k}} = -2t [\cos(k_x) + \cos(k_y)]$$

which is spin-invariant. The MFT description of the model reduces to a gas of free “ $\gamma$ -fermions”, described by the Nambu spinor of Eq. (4.7),

$$\hat{\Gamma}_{\mathbf{k}\sigma} = W_{\mathbf{k}\sigma} \hat{\Psi}_{\mathbf{k}\sigma} = \begin{bmatrix} \hat{\gamma}_{\mathbf{k}\sigma}^{(-)} \\ \hat{\gamma}_{\mathbf{k}\sigma}^{(+)} \end{bmatrix}$$

where

$$W_{\mathbf{k}\sigma} = \begin{bmatrix} -\sin \theta_{\mathbf{k}\sigma} & -\cos \theta_{\mathbf{k}\sigma} \\ \cos \theta_{\mathbf{k}\sigma} & -\sin \theta_{\mathbf{k}\sigma} \end{bmatrix} \quad \text{and} \quad \sin 2\theta_{\mathbf{k}\sigma} \equiv \frac{\Delta_{\sigma}}{E_{\mathbf{k}}}$$

These fermions populate the two bands  $\pm E_{\mathbf{k}} = \sqrt{\epsilon_{\mathbf{k}}^2 + \Delta^2}$ . The entire system is mapped onto an ensemble of pseudo-spins, each subject to a pseudo-field, as in Fig. 2.2. To diagonalize the system essentially means to align each pseudo-spin with the  $z$  axis. Within on the notation of Fig. 4.3, the following expectations values hold:

$$\langle \hat{\Psi}_{\mathbf{k}\sigma}^\dagger \tau^x \hat{\Psi}_{\mathbf{k}\sigma} \rangle = \sin(2\theta_{\mathbf{k}}) \langle \hat{\Gamma}_{\mathbf{k}\sigma}^\dagger \tau^z \hat{\Gamma}_{\mathbf{k}\sigma} \rangle \quad (2.8)$$

$$\langle \hat{\Psi}_{\mathbf{k}\sigma}^\dagger \tau^y \hat{\Psi}_{\mathbf{k}\sigma} \rangle = 0 \quad (2.9)$$

$$\langle \hat{\Psi}_{\mathbf{k}\sigma}^\dagger \tau^z \hat{\Psi}_{\mathbf{k}\sigma} \rangle = -\cos(2\theta_{\mathbf{k}}) \langle \hat{\Gamma}_{\mathbf{k}\sigma}^\dagger \tau^z \hat{\Gamma}_{\mathbf{k}\sigma} \rangle \quad (2.10)$$

and since the  $\gamma$ -fermions are free and in the rotated frame the pseudo-field points “up”,

$$\langle \hat{\Gamma}_{\mathbf{k}\sigma}^\dagger \tau^z \hat{\Gamma}_{\mathbf{k}\sigma} \rangle = \frac{1}{2} [f(-E_{\mathbf{k}}; \beta, \tilde{\mu}) - f(E_{\mathbf{k}}; \beta, \tilde{\mu})]$$



we get

$$\overbrace{-nV \sum_{\langle \mathbf{r}\mathbf{r}' \rangle} \sum_{\sigma} [\hat{n}_{\mathbf{r}'\sigma} + \hat{n}_{\mathbf{r}\sigma}] + mV \sum_{\langle \mathbf{r}\mathbf{r}' \rangle} \sum_{\sigma} (-1)^{\delta_{\sigma=\uparrow}} \left[ (-1)^{x'+y'} \hat{n}_{\mathbf{r}'\sigma} + (-1)^{x+y} \hat{n}_{\mathbf{r}\sigma} \right]}^{\text{s.s.}} \\ \underbrace{-nV \sum_{\langle \mathbf{r}\mathbf{r}' \rangle} \sum_{\sigma} [\hat{n}_{\mathbf{r}'\bar{\sigma}} + \hat{n}_{\mathbf{r}\sigma}] + mV \sum_{\langle \mathbf{r}\mathbf{r}' \rangle} \sum_{\sigma} \left[ (-1)^{x'+y'+\delta_{\bar{\sigma}=\uparrow}} \hat{n}_{\mathbf{r}'\bar{\sigma}} + (-1)^{x+y+\delta_{\sigma=\uparrow}} \hat{n}_{\mathbf{r}\sigma} \right]}_{\text{o.s.}}$$

For a square lattice, if  $\mathbf{r} = (x, y)$  and  $\mathbf{r}' = (x', y')$  are NNs evidently

$$(-1)^{x'+y'} = (-1)^{x+y+1}$$

Moreover,

$$(-1)^{\delta_{\bar{\sigma}=\uparrow}} = (-1)^{\delta_{\sigma=\uparrow}+1}$$

We obtain

$$\overbrace{-nV \sum_{\langle \mathbf{r}\mathbf{r}' \rangle} \sum_{\sigma} [\hat{n}_{\mathbf{r}\sigma} + \hat{n}_{\mathbf{r}'\sigma}]}^{\text{s.s. (density)}} + \overbrace{mV \sum_{\langle \mathbf{r}\mathbf{r}' \rangle} \sum_{\sigma} (-1)^{x+y+\delta_{\sigma=\uparrow}} [\hat{n}_{\mathbf{r}\sigma} - \hat{n}_{\mathbf{r}'\sigma}]}^{\text{s.s. (magnetization)}} \\ - \underbrace{nV \sum_{\langle \mathbf{r}\mathbf{r}' \rangle} \sum_{\sigma} [\hat{n}_{\mathbf{r}\sigma} + \hat{n}_{\mathbf{r}'\bar{\sigma}}]}_{\text{o.s. (density)}} + \underbrace{mV \sum_{\langle \mathbf{r}\mathbf{r}' \rangle} \sum_{\sigma} (-1)^{x+y+\delta_{\sigma=\uparrow}} [\hat{n}_{\mathbf{r}\sigma} + \hat{n}_{\mathbf{r}'\bar{\sigma}}]}_{\text{o.s. (magnetization)}} \quad (2.15)$$

In the above expressions the various contribution have been separated in “density” contributions and “magnetization” contributions. Let me deal with these separately.

**Density terms.** Consider the *s.s.* and *o.s.* (density) terms of Expr. (2.15). Since

$$\sum_{\langle \mathbf{r}\mathbf{r}' \rangle} \sum_{\sigma} [\hat{n}_{\mathbf{r}\sigma} + \hat{n}_{\mathbf{r}'\sigma}] = \sum_{\langle \mathbf{r}\mathbf{r}' \rangle} \sum_{\sigma} [\hat{n}_{\mathbf{r}\sigma} + \hat{n}_{\mathbf{r}'\bar{\sigma}}] = z\hat{N}$$

with  $z = 4$  the lattice coordination factor, indicating the number of NNs per site, then the first and third terms of Expr. (2.15) contribute to a pure chemical potential shift. The renormalized chemical potential is:

$$\tilde{\mu} \equiv \mu + 2znV \quad (2.16)$$

**Magnetization terms.** The *s.s.* and *o.s.* (magnetization) terms of Expr. (2.15) are to be reduced to a renormalization of the gap function. Explicitly,

$$mV \sum_{\langle \mathbf{r}\mathbf{r}' \rangle} \sum_{\sigma} (-1)^{x+y+\delta_{\sigma=\uparrow}} [\hat{n}_{\mathbf{r}\sigma} - \hat{n}_{\mathbf{r}'\sigma}] + mV \sum_{\langle \mathbf{r}\mathbf{r}' \rangle} \sum_{\sigma} (-1)^{x+y+\delta_{\sigma=\uparrow}} [\hat{n}_{\mathbf{r}\sigma} + \hat{n}_{\mathbf{r}'\bar{\sigma}}] \\ = -2zmV \sum_{\mathbf{r}} (-1)^{x+y} [\hat{n}_{\mathbf{r}\uparrow} - \hat{n}_{\mathbf{r}\downarrow}] \quad (2.17)$$

Consider now the last term of the pure Hubbard model under MFT approximations of Eq. (4.2),

$$-mU \sum_{\mathbf{r}} (-1)^{x+y} [\hat{n}_{\mathbf{r}\uparrow} - \hat{n}_{\mathbf{r}\downarrow}] \quad (\text{Local gap})$$

Expr. (2.17) is formally identical, thus we obtain a contribution to the renormalization of the AF gap,

$$\Delta \rightarrow \Delta + 2zmV + (\text{s.s. contribution}) \quad (2.18)$$

This, together with Eq. (2.16), concludes the non-local Hartree reparametrization of the hamiltonian. Next section is devoted to analyzing the effect of the Fock term.

### 2.2.2 Fock renormalization of the hopping amplitude

From Wick's decomposition of  $\hat{H}_V$ , the only allowed Fock term comes from the same-spin part due to SU(2) symmetry selection rules. Said hamiltonian term is

$$V \sum_{\langle ij \rangle} \sum_{\sigma} \left[ \langle \hat{c}_{i\sigma}^{\dagger} \hat{c}_{j\sigma} \rangle \hat{c}_{j\sigma}^{\dagger} \hat{c}_{i\sigma} + \text{h.c.} \right] \quad (2.19)$$

(note the + sign in front of it). A bond-wise hopping amplitude can be defined,

$$\tilde{t}_{ij\sigma} \equiv t - V \langle \hat{c}_{j\sigma}^{\dagger} \hat{c}_{i\sigma} \rangle$$

In the AF phase, given some site  $i$  and a spin  $\sigma$ , evidently  $\tilde{t}_{ij\sigma}$  must be identical for any NN site  $j$ . Over the planar square lattice, this implies that the quantity  $\langle \hat{c}_{j\sigma}^{\dagger} \hat{c}_{i\sigma} \rangle$  exhibits  $s^*$ -wave symmetry (also referred to as "Extended  $s$ -wave symmetry"). Later in the text, different symmetry structures will be discussed thoroughly. For now, the  $s^*$ -wave symmetry is the one given in Tab. 2.1 and depicted in Fig. 2.4b. These considerations will become useful later. The effective diffusive hamiltonian is given by

$$\begin{aligned} \hat{H}_{\tilde{t}} &= \hat{H}_t + V \sum_{\langle ij \rangle} \sum_{\sigma} \left[ \langle \hat{c}_{i\sigma}^{\dagger} \hat{c}_{j\sigma} \rangle \hat{c}_{j\sigma}^{\dagger} \hat{c}_{i\sigma} + \text{h.c.} \right] \\ &= - \sum_{\langle ij \rangle} \sum_{\sigma} \left[ \tilde{t}_{ij\sigma} \hat{c}_{i\sigma}^{\dagger} \hat{c}_{j\sigma} + \text{h.c.} \right] \end{aligned}$$

As will become clear in next section, not only the diffusive part of the hamiltonian actually is affected by the Fock renormalization; also the gap terms are effectively renormalized.

In reciprocal space, the effective hopping must be transformed as well. Consider the Fourier Transform given in Eq. (2.4), applied to Eq. (2.19),

$$\begin{aligned} V \sum_{\langle ij \rangle} \sum_{\sigma} \left[ \langle \hat{c}_{i\sigma}^{\dagger} \hat{c}_{j\sigma} \rangle \hat{c}_{j\sigma}^{\dagger} \hat{c}_{i\sigma} + \text{h.c.} \right] \\ = \frac{2V}{L_x L_y} \sum_{\mathbf{K}, \mathbf{k}, \mathbf{k}'} \sum_{\sigma} [\cos(\delta k_x) + \cos(\delta k_y)] \langle \hat{c}_{\mathbf{K}+\mathbf{k}\sigma}^{\dagger} \hat{c}_{\mathbf{K}-\mathbf{k}'\sigma} \rangle \hat{c}_{\mathbf{K}-\mathbf{k}\sigma}^{\dagger} \hat{c}_{\mathbf{K}+\mathbf{k}'\sigma} \quad (2.20) \end{aligned}$$

where the 2 prefactor comes from recognizing that the h.c. generates an identical contribution to the full sum. In order to proceed, it is now necessary to understand how the AF phase is realized in reciprocal space. As is exposed in App. 4, to impose an AF Ansatz of the form

$$\langle \hat{n}_{\mathbf{r}\sigma} \rangle = n - (-1)^{x+y+\delta_{\sigma=\uparrow}} m$$

leads to an AF ground-state of free fermions at temperature  $\beta$  described by the Nambu spinor of Eq. (4.7). All parameters are renormalized, thus we must account for renormalized band energies  $\pm \tilde{E}_{\mathbf{k}\sigma}$  as well. The ground-state is realized by simply populating the two bands  $\pm \tilde{E}_{\mathbf{k}\sigma}$  as

$$\bigotimes_{\mathbf{k} \in \text{MBZ}} \bigotimes_{\sigma} \left[ \left( \hat{\gamma}_{\mathbf{k}\sigma}^{(-)} \right)^{\dagger} f(-\tilde{E}_{\mathbf{k}}; \beta, \mu) + \left( \hat{\gamma}_{\mathbf{k}\sigma}^{(+)} \right)^{\dagger} f(\tilde{E}_{\mathbf{k}}; \beta, \mu) \right] |\Omega\rangle$$

The  $\hat{\gamma}$  operators are normalized superpositions of two  $\hat{c}$  operators at points in reciprocal space separated by a  $\pi$  shift. It follows that the above state is ultimately a superposition of many-body pure states, each of which has either the  $\mathbf{k}\sigma$  state occupied or the  $\mathbf{k} + \pi\sigma$  state for each  $\mathbf{k} \in \text{MBZ}$ ,  $\sigma \in \{\uparrow, \downarrow\}$ . It follows that, when computing generically  $\langle \hat{c}_{\mathbf{k}_1\sigma}^{\dagger} \hat{c}_{\mathbf{k}_2\sigma} \rangle$ , such expectation value can be non-zero if and only if  $\mathbf{k}_1 = \mathbf{k}_2 + n\pi$ , being  $n \in \mathbb{Z}$ . Going back to Eq. (2.20), this implies only two contributions are non-zero:

$$\mathbf{k} = -\mathbf{k}' \quad \text{or} \quad \mathbf{k} + \pi = -\mathbf{k}'$$



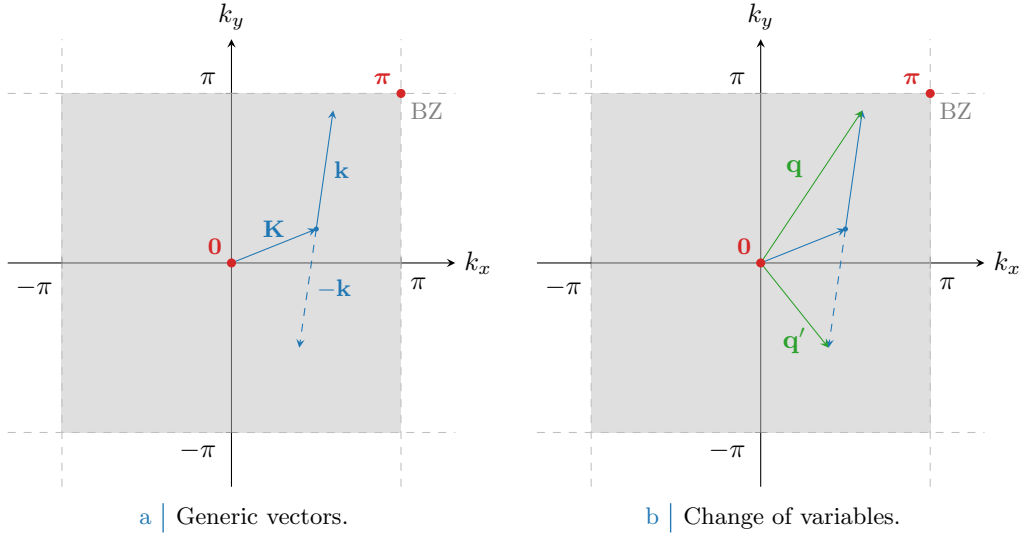


**Figure 2.3** Representation of the vectors involved in the diagonal terms of Eq. (2.21). In Fig. 2.3a generic vectors are considered, cycling over all values of  $\mathbf{K}, \mathbf{k} \in \text{BZ}$ . In Fig. 2.3b is depicted the variables change to the new vectors  $\mathbf{q}, \mathbf{q}'$ .

Then Eq. (2.20) is reduced to:

$$\frac{2V}{L_x L_y} \sum_{\mathbf{K}, \mathbf{k}} \sum_{\sigma} [\cos(2k_x) + \cos(2k_y)] \left[ \underbrace{\langle \hat{c}_{\mathbf{K}+\mathbf{k}\sigma}^\dagger \hat{c}_{\mathbf{K}+\mathbf{k}\sigma} \rangle \hat{c}_{\mathbf{K}-\mathbf{k}\sigma}^\dagger \hat{c}_{\mathbf{K}-\mathbf{k}\sigma}}_{\text{Diagonal terms}} - \underbrace{\langle \hat{c}_{\mathbf{K}+\mathbf{k}\sigma}^\dagger \hat{c}_{\mathbf{K}+\mathbf{k}+\pi\sigma} \rangle \hat{c}_{\mathbf{K}-\mathbf{k}\sigma}^\dagger \hat{c}_{\mathbf{K}-\mathbf{k}-\pi\sigma}}_{\text{Off-diagonal terms}} \right] \quad (2.21)$$

Now, the above equation presents *diagonal* and *off-diagonal* terms. Let me discuss them separately.

**Diagonal terms.** The diagonal terms of Eq. (2.21) are simple density interactions with the mean density field. Consider Fig. 2.3a: density at vector  $\mathbf{q} \equiv \mathbf{K} + \mathbf{k}$  interacts with the mean density at vector  $\mathbf{q}' \equiv \mathbf{K} - \mathbf{k}$ . These variables are depicted in Fig. 2.3b. Apply the variable change in the diagonal part of Eq. (2.21),

$$\begin{aligned} \frac{2V}{L_x L_y} \sum_{\mathbf{q}, \mathbf{q}'} \sum_{\sigma} [\cos(2k_x) + \cos(2k_y)] \langle \hat{c}_{\mathbf{K}+\mathbf{k}\sigma}^\dagger \hat{c}_{\mathbf{K}+\mathbf{k}\sigma} \rangle \hat{c}_{\mathbf{K}-\mathbf{k}\sigma}^\dagger \hat{c}_{\mathbf{K}-\mathbf{k}\sigma} \\ = \frac{2V}{L_x L_y} \sum_{\mathbf{q}, \mathbf{q}'} \sum_{\sigma} [\cos(\delta q_x) + \cos(\delta q_y)] \langle \hat{c}_{\mathbf{q}\sigma}^\dagger \hat{c}_{\mathbf{q}\sigma} \rangle \hat{c}_{\mathbf{q}'\sigma}^\dagger \hat{c}_{\mathbf{q}'\sigma} \end{aligned} \quad (2.22)$$

being for  $\ell = x, y$

$$\begin{aligned} \delta q_\ell &\equiv q_\ell - q'_\ell \\ &= (K_\ell + k_\ell) - (K_\ell - k_\ell) \\ &= 2k_\ell \end{aligned}$$

Decompose the form factor,

$$\begin{aligned} \cos(\delta q_x) + \cos(\delta q_y) &= \frac{1}{2}(\cos q_x + \cos q_y)(\cos q'_x + \cos q'_y) && (s^*\text{-wave}) \\ &+ \sin q_x \sin q'_x && (p_x\text{-wave}) \\ &+ \sin q_y \sin q'_y && (p_y\text{-wave}) \\ &+ \frac{1}{2}(\cos q_x - \cos q_y)(\cos q'_x - \cos q'_y) && (d_{x^2-y^2}\text{-wave}) \end{aligned}$$

where all contributions are classified by their symmetry structure. These structure are listed and then later on dealt with in Tab. 2.2, in the context of anisotropic pairing and topological superconductivity. For now, all that matters is that, in the AF phase,  $\langle \hat{c}_{\mathbf{q}\sigma}^\dagger \hat{c}_{\mathbf{q}\sigma} \rangle$  must be  $s^*$ -wave symmetric, as anticipated in the starting discussion of Sec. 2.2.2. This is due to the fact that of the four symmetries listed above, only the first one exhibits both  $x, y$  reflections symmetry and  $\pi/2$  rotational invariance. It follows, only the  $s^*$ -wave component when coupled to  $\langle \hat{c}_{\mathbf{q}\sigma}^\dagger \hat{c}_{\mathbf{q}\sigma} \rangle$  in Eq. (2.22) gives a non-null contribution, reducing the latter to

$$\begin{aligned} \frac{2V}{L_x L_y} \sum_{\mathbf{q}, \mathbf{q}'} \sum_{\sigma} [\cos(\delta q_x) + \cos(\delta q_y)] \langle \hat{c}_{\mathbf{q}\sigma}^\dagger \hat{c}_{\mathbf{q}\sigma} \rangle \hat{c}_{\mathbf{q}'\sigma}^\dagger \hat{c}_{\mathbf{q}'\sigma} \\ = \frac{V}{L_x L_y} \sum_{\mathbf{q}'\sigma} (\cos q'_x + \cos q'_y) \hat{c}_{\mathbf{q}'\sigma}^\dagger \hat{c}_{\mathbf{q}'\sigma} \sum_{\mathbf{q}} (\cos q_x + \cos q_y) \langle \hat{c}_{\mathbf{q}\sigma}^\dagger \hat{c}_{\mathbf{q}\sigma} \rangle \end{aligned} \quad (2.23)$$

Note that, for two vectors separated by a  $\pi$  shift,

$$\cos q_x + \cos q_y = -\cos(q_x + \pi) - \cos(q_y + \pi)$$

Because of this feature, changing the variables names  $\mathbf{q}' \rightarrow \mathbf{k}$ ,  $\mathbf{q} \rightarrow \mathbf{k}'$  for the sake of general aesthetic coherence, it becomes evident that the above equation gives the bands renormalization:

$$\begin{aligned} \epsilon_{\mathbf{k}} &\equiv -2t (\cos k_x + \cos k_y) \\ \tilde{\epsilon}_{\mathbf{k}} &\equiv \epsilon_{\mathbf{k}} + \left[ \frac{1}{2L_x L_y} \sum_{\mathbf{k}'} (\cos k'_x + \cos k'_y) \langle \hat{c}_{\mathbf{k}'\sigma}^\dagger \hat{c}_{\mathbf{k}'\sigma} \rangle \right] \times 2V (\cos k_x + \cos k_y) \end{aligned}$$

Note that on the left-hand side  $\tilde{\epsilon}_{\mathbf{k}}$  is independent of  $\sigma$ . To explain this, let:

$$w_{\sigma}^{(0)} \equiv \frac{1}{2L_x L_y} \sum_{\mathbf{k} \in \text{BZ}} (\cos k_x + \cos k_y) \langle \hat{c}_{\mathbf{k}\sigma}^\dagger \hat{c}_{\mathbf{k}\sigma} \rangle$$

By simple symmetry considerations, it must be  $\langle \hat{c}_{\mathbf{k}\uparrow}^\dagger \hat{c}_{\mathbf{k}\uparrow} \rangle = \langle \hat{c}_{\mathbf{k}\downarrow}^\dagger \hat{c}_{\mathbf{k}\downarrow} \rangle$  (as is later seen explicitly). Then,

$$w_{\uparrow}^{(0)} = w_{\downarrow}^{(0)} \equiv w^{(0)}$$

The computation can be simplified:

$$\begin{aligned} w^{(0)} &= \frac{1}{2L_x L_y} \sum_{\mathbf{k} \in \text{BZ}} (\cos k_x + \cos k_y) \langle \hat{c}_{\mathbf{k}\uparrow}^\dagger \hat{c}_{\mathbf{k}\uparrow} \rangle \\ &= \frac{1}{2L_x L_y} \sum_{\mathbf{k} \in \text{MBZ}} (\cos k_x + \cos k_y) \langle \hat{c}_{\mathbf{k}\uparrow}^\dagger \hat{c}_{\mathbf{k}\uparrow} - \hat{c}_{\mathbf{k}+\pi\uparrow}^\dagger \hat{c}_{\mathbf{k}+\pi\uparrow} \rangle \\ &= \frac{1}{2L_x L_y} \sum_{\mathbf{k} \in \text{MBZ}} (\cos k_x + \cos k_y) \langle \hat{\Psi}_{\mathbf{k}\uparrow}^\dagger \tau^z \hat{\Psi}_{\mathbf{k}\uparrow} \rangle \\ &= -\frac{1}{4L_x L_y} \sum_{\mathbf{k} \in \text{MBZ}} (\cos k_x + \cos k_y) \frac{\tilde{\epsilon}_{\mathbf{k}}}{\tilde{E}_{\mathbf{k}}} \left[ f(-\tilde{E}_{\mathbf{k}}; \beta, \tilde{\mu}) - f(\tilde{E}_{\mathbf{k}}; \beta, \tilde{\mu}) \right] \end{aligned} \quad (2.24)$$

where in the second passage the sign change is due to the presence of the structure factor, and in the fourth passage Eq. (2.13) and the relations (2.14) have been used. It follows, finally, that the hopping parameter gets effectively renormalized:

$$\tilde{t} \equiv t - w^{(0)} V \quad (2.25)$$

The full effective MFT hamiltonian is spin-independent, then similarly the renormalized parameters cannot exhibit spin dependency. This justifies the fact that  $\tilde{t}$  is spin-independent, and so is  $\tilde{\epsilon}_{\mathbf{k}}$ .

**Off-diagonal terms.** Consider the off-diagonal terms of Eq. (2.21). These contribute instead to the gap renormalization, being out of diagonal in the  $2 \times 2$  hamiltonian matrix. Define  $\mathbf{q}, \mathbf{q}'$  as in Fig. 2.3b, and rewrite

$$\begin{aligned} -\frac{2V}{L_x L_y} \sum_{\mathbf{K}, \mathbf{k}} \sum_{\sigma} [\cos(2k_x) + \cos(2k_y)] \langle \hat{c}_{\mathbf{K}+\mathbf{k}\sigma}^\dagger \hat{c}_{\mathbf{K}+\mathbf{k}+\pi\sigma} \rangle \hat{c}_{\mathbf{K}-\mathbf{k}\sigma}^\dagger \hat{c}_{\mathbf{K}-\mathbf{k}-\pi\sigma} \\ = -\frac{2V}{L_x L_y} \sum_{\mathbf{q}} \langle \hat{c}_{\mathbf{q}\sigma}^\dagger \hat{c}_{\mathbf{q}+\pi\sigma} \rangle \sum_{\mathbf{q}'\sigma} [\cos(\delta q_x) + \cos(\delta q_y)] \hat{c}_{\mathbf{q}'\sigma}^\dagger \hat{c}_{\mathbf{q}'+\pi\sigma} \end{aligned}$$

Identical considerations about the  $s^*$ -wave symmetry structure of the expectation value  $\langle \hat{c}_{\mathbf{q}\sigma}^\dagger \hat{c}_{\mathbf{q}+\pi\sigma} \rangle$  as in the above paragraph hold. Once again renaming the variables  $\mathbf{q}' \rightarrow \mathbf{k}, \mathbf{q} \rightarrow \mathbf{k}'$  for the sake of general aesthetic coherence, this gives

$$\begin{aligned} -\frac{2V}{L_x L_y} \sum_{\mathbf{K}, \mathbf{k}} \sum_{\sigma} [\cos(2k_x) + \cos(2k_y)] \langle \hat{c}_{\mathbf{K}+\mathbf{k}\sigma}^\dagger \hat{c}_{\mathbf{K}+\mathbf{k}+\pi\sigma} \rangle \hat{c}_{\mathbf{K}-\mathbf{k}\sigma}^\dagger \hat{c}_{\mathbf{K}-\mathbf{k}-\pi\sigma} \\ = -2V \left[ \frac{1}{2L_x L_y} \sum_{\mathbf{k}'} (\cos k'_x + \cos k'_y) \langle \hat{c}_{\mathbf{k}'\sigma}^\dagger \hat{c}_{\mathbf{k}'+\pi\sigma} \rangle \right] \sum_{\mathbf{k}\sigma} (\cos k_x + \cos k_y) \hat{c}_{\mathbf{k}\sigma}^\dagger \hat{c}_{\mathbf{k}+\pi\sigma} \quad (2.26) \end{aligned}$$

Because of this, the  $x$  component of the pseudo-magnetic field – the gap already renormalized by Eq. (2.18) when analyzing o.s. terms – takes up another renormalization contribution, finally giving

$$\tilde{\Delta}_{\mathbf{k}\sigma} \equiv m(U + 2zV) \times (-1)^{\delta_{\sigma=\uparrow}} + i2V w_{\sigma}^{(\pi)} (\cos k_x + \cos k_y) \quad (2.27)$$

where

$$w_{\sigma}^{(\pi)} \equiv -\frac{i}{2L_x L_y} \sum_{\mathbf{k} \in \text{BZ}} (\cos k_x + \cos k_y) \langle \hat{c}_{\mathbf{k}\sigma}^\dagger \hat{c}_{\mathbf{k}+\pi\sigma} \rangle$$

As will be clear in few lines,  $w_{\sigma}^{(\pi)}$  as is defined here is purely real (due to the presence of a  $-i$  prefactor). This makes  $\tilde{\Delta}_{\mathbf{k}\sigma}$  made of two contributions,

$$\text{Re}\{\tilde{\Delta}_{\mathbf{k}\sigma}\} = m(U + 2zV) \times (-1)^{\delta_{\sigma=\uparrow}} \quad \text{Im}\{\tilde{\Delta}_{\mathbf{k}\sigma}\} = 2V w_{\sigma}^{(\pi)} (\cos k_x + \cos k_y)$$

Now, since the gapped band value cannot depend on the spin index for symmetry reasons,

$$\tilde{E}_{\mathbf{k}} = \sqrt{\tilde{\epsilon}_{\mathbf{k}}^2 + |\tilde{\Delta}_{\mathbf{k}\sigma}|^2}$$

this implies necessarily  $|\tilde{\Delta}_{\mathbf{k}\uparrow}| = |\tilde{\Delta}_{\mathbf{k}\downarrow}|$ . This is possible either if  $w_{\uparrow}^{(\pi)} = \pm w_{\downarrow}^{(\pi)}$ . Actually, in the end the exact sign does not matter: all that matters is the gap amplitude  $|\tilde{\Delta}_{\mathbf{k}\sigma}|$ , thus we may restrict to  $\sigma = \uparrow$  and omit from now on the spin index. [ Not so sure about this. ]. This then gives us the final result for the renormalized gap function,

$$\tilde{\Delta}_{\mathbf{k}} \equiv m(U + 2zV) + 2i w^{(\pi)} V (\cos k_x + \cos k_y) \quad (2.28)$$

This result, together with Eqns. (2.16) and (2.25), concludes the renormalization of all parameters due to the non-local interaction. To calculate  $w^{(\pi)}$  self consistently, we may use:

$$\begin{aligned} w^{(\pi)} &= -\frac{i}{2L_x L_y} \sum_{\mathbf{k} \in \text{BZ}} (\cos k_x + \cos k_y) \langle \hat{c}_{\mathbf{k}\uparrow}^\dagger \hat{c}_{\mathbf{k}+\pi\uparrow} \rangle \\ &= -\frac{i}{2L_x L_y} \sum_{\mathbf{k} \in \text{MBZ}} (\cos k_x + \cos k_y) \langle \hat{c}_{\mathbf{k}\uparrow}^\dagger \hat{c}_{\mathbf{k}+\pi\uparrow} - \hat{c}_{\mathbf{k}+\pi\uparrow}^\dagger \hat{c}_{\mathbf{k}\uparrow} \rangle \\ &= \frac{1}{2L_x L_y} \sum_{\mathbf{k} \in \text{MBZ}} (\cos k_x + \cos k_y) \langle \hat{\Psi}_{\mathbf{k}\uparrow}^\dagger \tau^y \hat{\Psi}_{\mathbf{k}\uparrow} \rangle \\ &= \frac{1}{4L_x L_y} \sum_{\mathbf{k} \in \text{MBZ}} (\cos k_x + \cos k_y) \frac{\text{Im}\{\tilde{\Delta}_{\mathbf{k}}\}}{\tilde{E}_{\mathbf{k}}} \left[ f(-\tilde{E}_{\mathbf{k}}; \beta, \tilde{\mu}) - f(\tilde{E}_{\mathbf{k}}; \beta, \tilde{\mu}) \right] \quad (2.29) \end{aligned}$$

Notice that this expression is purely real, as promised, and contributes to the  $y$  component of the pseudo-field of Fig. 2.2.

### 2.2.3 Renormalized hamiltonian behavior

Summing up, the non-local interaction  $\hat{H}_V$  when discussed within MFT affects the EHM hamiltonian by renormalizing the various parameters as:

$$\begin{aligned}\tilde{\mu} &\equiv \mu + 2znV \\ \tilde{t} &\equiv t - w^{(0)}V \\ \tilde{\Delta}_{\mathbf{k}} &\equiv m(U + 2zV) + 2iw^{(\pi)}V [\cos(k_x) + \cos(k_y)]\end{aligned}$$

Various details are to be noted. First, the non-local interaction both contributes by enlarging the real part of the gap [ **To be understood: why does a non-local attraction increase the gap?** ] as well as introducing a  $s^*$ -wave shaped imaginary gap. Interestingly, if

$$\left(w^{(0)}\right)^{-1} = V/t$$

the diffusive part of the hamiltonian drops to zero. For even larger values, diffusion becomes energetically expensive and  $V$ -induced localization appears.

The new set of Hartree-Fock parameters to be determined is given by the vector

$$\mathbf{v} \equiv \begin{bmatrix} m \\ w^{(0)} \\ w^{(\pi)} \end{bmatrix}$$

Its three components are self-consistently determined by Eqns. (2.24) and (2.29). The self-consistent equation for  $m$  comes from Eq. (4.13), and reads

$$\begin{aligned}m &= \frac{1}{2L_x L_y} \sum_{\mathbf{k} \in \text{BZ}} \langle \hat{c}_{\mathbf{k}\uparrow}^\dagger \hat{c}_{\mathbf{k}+\pi\uparrow} - \hat{c}_{\mathbf{k}\downarrow}^\dagger \hat{c}_{\mathbf{k}+\pi\downarrow} \rangle \\ &= \frac{1}{2L_x L_y} \sum_{\mathbf{k} \in \text{MBZ}} \langle \hat{\Psi}_{\mathbf{k}\uparrow}^\dagger \tau^x \hat{\Psi}_{\mathbf{k}\uparrow} - \hat{\Psi}_{\mathbf{k}\downarrow}^\dagger \tau^x \hat{\Psi}_{\mathbf{k}\downarrow} \rangle \\ &= \frac{1}{L_x L_y} \sum_{\mathbf{k} \in \text{MBZ}} \langle \hat{\Psi}_{\mathbf{k}\uparrow}^\dagger \tau^x \hat{\Psi}_{\mathbf{k}\uparrow} \rangle \\ &= \frac{1}{L_x L_y} \sum_{\mathbf{k} \in \text{MBZ}} \frac{\text{Re}\{\tilde{\Delta}_{\mathbf{k}}\}}{\tilde{E}_{\mathbf{k}}} \left[ f(-\tilde{E}_{\mathbf{k}}; \beta, \tilde{\mu}) - f(\tilde{E}_{\mathbf{k}}; \beta, \tilde{\mu}) \right]\end{aligned}\tag{2.30}$$

In the second passage  $\langle \hat{\Psi}_{\mathbf{k}\uparrow}^\dagger \tau^x \hat{\Psi}_{\mathbf{k}\uparrow} \rangle = -\langle \hat{\Psi}_{\mathbf{k}\downarrow}^\dagger \tau^x \hat{\Psi}_{\mathbf{k}\downarrow} \rangle$  has been used. In the third passage, relations (2.14) were inserted. The algorithm sketched in Sec. 4.2.2 remains essentially identical, with the *caveat* of defining three HF parameters, running for each a convergence analysis.

### 2.2.4 Results of the HF algorithm

An HF algorithm similar to the one sketched in Sec. 4.2.2 was run, now self-consistently on the entire HF vector  $\mathbf{v}$ . [ **Insert results of analysis.** ]

## 2.3 Superconducting instability

This section is devoted to studying the superconducting phase of the system. The only symmetry we assume to break is the  $U(1)$  charge symmetry, thus allowing for superconducting fluctuations. As is described thoroughly in Sec. 2.2.2, the hopping amplitude is renormalized because of the non-local attraction. The symmetry structure of the pairing mechanism determines the contributing Cooper fluctuations: for  $s$ -wave and  $d$ -wave superconductivity, only the o.s. Cooper term contributes; for  $p_\ell$ -wave superconductivity, the s.s. term contributes as well. In the following sections, a derivation containing both Cooper terms is proposed.

[ **To be continued: separate singlet and triplet pairing channels, and describe them separately by the means of four-components Nambu spinors. Use selection rules to set  $\Delta^{(p_\ell)} = 0$  in the singlet channel, in order to justify results obtained by a pure space-even simulation containing just the o.s. terms.** ]

### 2.3.1 Mean-field treatment of the non-local term

This approach leads to the conclusion that the (coherent) ground-state of the system must be an eigenstate of the mean-field effective hamiltonian:

$$\begin{aligned}\hat{H}^{(e)} = & -t \sum_{\langle ij \rangle} \sum_{\sigma} \hat{c}_{i\sigma}^{\dagger} \hat{c}_{j\sigma} + U \sum_{i \in \mathcal{S}} \hat{n}_{i\uparrow} \hat{n}_{i\downarrow} \\ & - V \sum_{i \in \mathcal{S}} \sum_{\ell=x,y} \sum_{\delta=\pm\delta_{\ell}} \left[ \langle \hat{c}_{i\uparrow}^{\dagger} \hat{c}_{i+\delta\downarrow}^{\dagger} \rangle \hat{c}_{i+\delta\downarrow} \hat{c}_{i\uparrow} + \text{h.c.} \right]\end{aligned}\quad (2.31)$$

Note that I am here summing over  $i \in \mathcal{S}$ : this is the same as considering both the  $\uparrow\downarrow$  *plus* the  $\downarrow\uparrow$  terms of the o.s. hamiltonian involved in even-wave pairing. The pairing correlation function is defined across each bond as the pairing expectation

$$g_{ij} \equiv \langle \hat{c}_{i\uparrow}^{\dagger} \hat{c}_{j\downarrow}^{\dagger} \rangle$$

The effective hamiltonian reads:

$$\hat{H}^{(e)} = -t \sum_{\langle ij \rangle} \sum_{\sigma} \hat{c}_{i\sigma}^{\dagger} \hat{c}_{j\sigma} + U \sum_{i \in \mathcal{S}} \hat{n}_{i\uparrow} \hat{n}_{i\downarrow} - V \sum_{\langle ij \rangle} \left[ g_{ij} \hat{c}_{j\downarrow} \hat{c}_{i\uparrow} + g_{ij}^* \hat{c}_{i\uparrow}^{\dagger} \hat{c}_{j\downarrow}^{\dagger} \right] \quad (2.32)$$

As in standard BCS theory, this hamiltonian – being quadratic in the electronic operators – can be diagonalized via a Bogoliubov rotation. Superconducting pairing can arise both from the local  $U$  term and from the non-local  $V$  term. In next sections it is assumed the  $V$  term generates dominant superconductivity via its weak non-local pairing.

### 2.3.2 Mean-field treatment of the local term

The mean-field description of the local (on-site)  $U$  interaction is given in detail in App. 4, along with a simple numerical analysis of the insurgence of antiferromagnetic ordering in a Hartree-Fock approximation scheme. Here the Cooper pairing is likewise assumed to dominate. Performing an analysis analogous to the one carried out in last section, we get the decoupling

$$U \sum_{i \in \mathcal{S}} \hat{n}_{i\uparrow} \hat{n}_{i\downarrow} \simeq U \sum_{i\sigma} \left[ f_i \hat{c}_{i\downarrow} \hat{c}_{i\uparrow} + f_i^* \hat{c}_{i\uparrow}^{\dagger} \hat{c}_{i\downarrow}^{\dagger} \right]$$

being

$$f_i \equiv \langle \hat{c}_{i\uparrow}^{\dagger} \hat{c}_{i\downarrow}^{\dagger} \rangle$$

Collect  $f$  and  $g$  in the unique function of two variables:

$$C(i, j) = \begin{cases} f_i & \text{if } i = j \\ g_{ij} & \text{if } |i - j| = 1 \\ (\dots) & \text{otherwise} \end{cases}$$

which expresses the generic correlator  $\langle \hat{c}_{i\uparrow}^{\dagger} \hat{c}_{j\downarrow}^{\dagger} \rangle$ . The correlator for  $|i - j| > 1$  is left unexpressed, and supposed to be subdominant. The decoupled hamiltonian, apart from pure energy shifts and suppressed terms, is given by

$$\begin{aligned}\hat{H}^{(e)} = & -t \sum_{\langle ij \rangle} \sum_{\sigma} \hat{c}_{i\sigma}^{\dagger} \hat{c}_{j\sigma} + U \sum_i \left[ f_i \hat{c}_{i\downarrow} \hat{c}_{i\uparrow} + f_i^* \hat{c}_{i\uparrow}^{\dagger} \hat{c}_{i\downarrow}^{\dagger} \right] \\ & - V \sum_{\langle ij \rangle} \left[ g_{ij} \hat{c}_{j\downarrow} \hat{c}_{i\uparrow} + g_{ij}^* \hat{c}_{i\uparrow}^{\dagger} \hat{c}_{j\downarrow}^{\dagger} \right]\end{aligned}\quad (2.33)$$

Next section is devoted to analyzing the consequences of choosing a specific topology (which is, symmetry structure) for the pairing correlations.

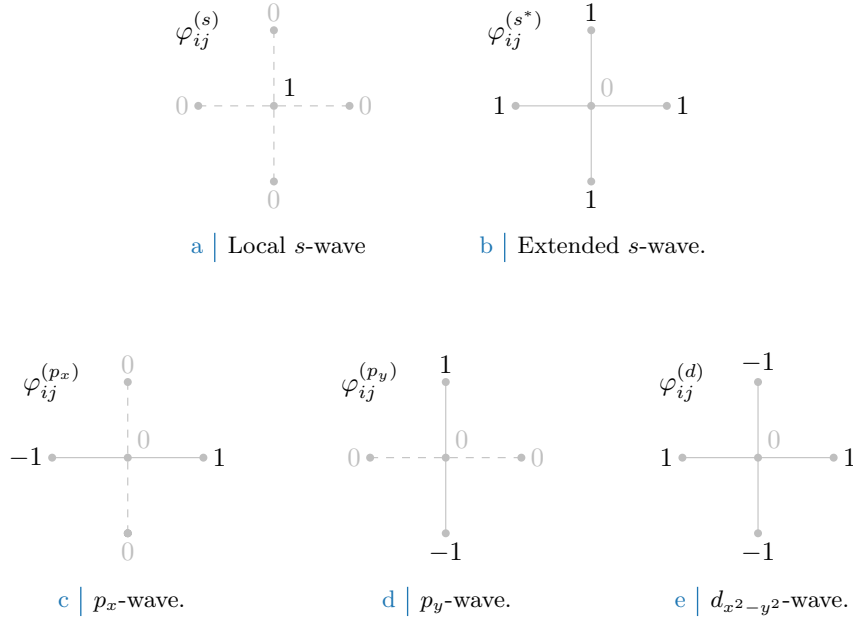


**Figure 2.4** | Form factors at different topologies, as listed in Tab. 2.1. In figures five sites are represented: the hub site  $i$  and its four NN. Solid lines represent non-zero values for  $\varphi_{\delta}$ , while dashed lines represent vanishing factors.

Structure	Form factor	Graph
$s$ -wave	$\varphi_{ij}^{(s)} = \delta_{ij}$	Fig. 2.4a
Extended $s$ -wave	$\varphi_{ij}^{(s^*)} = \delta_{j=i+\delta_x} + \delta_{j=i-\delta_x} + \delta_{j=i+\delta_y} + \delta_{j=i-\delta_y}$	Fig. 2.4b
$p_x$ -wave	$\varphi_{ij}^{(p_x)} = \delta_{j=i+\delta_x} - \delta_{j=i-\delta_x}$	Fig. 2.4c
$p_y$ -wave	$\varphi_{ij}^{(p_y)} = \delta_{j=i+\delta_y} - \delta_{j=i-\delta_y}$	Fig. 2.4d
$d_{x^2-y^2}$ -wave	$\varphi_{ij}^{(d)} = \delta_{j=i+\delta_x} + \delta_{j=i-\delta_x} - \delta_{j=i+\delta_y} - \delta_{j=i-\delta_y}$	Fig. 2.4e

**Table 2.1** | First four spatial structures for the correlation function  $C(i, j)$ . In the middle column, all spatial dependence is included in the  $\delta$ s, while  $f^s, g^{(\gamma)} \in \mathbb{C}$ . The last column indicates the graph representation of each contribution given in Fig. ???. Subscript  $x^2 - y^2$  is omitted for notational clarity.

### 2.3.3 Topological correlations

Topology plays an important role in establishing SC, giving rise to anisotropic pairing as well as real space structures for the Cooper pairs. The correlator  $g_{ij}$  is a function of position, specifically of its variables difference  $\delta \equiv \mathbf{x}_j - \mathbf{x}_i$ . Over the square lattice with NN interaction, the latter can assume four values:  $\delta = \pm\delta_x, \pm\delta_y$ . For a function of space defined over the four rim sites  $\mathbf{x}_i \pm \delta_\ell$  of Fig. 2.1, various symmetry structures can be defined under the planar rotations group  $\text{SO}(2)$ . In other words, the function  $g_\delta$  can be decomposed in planar harmonics (which are simply the sine-cosine basis). Equivalently, given two NN sites  $i, j$

$$g_{ij} = \sum_{\gamma} g^{(\gamma)} \varphi_{ij}^{(\gamma)}$$

where  $g^{(\gamma)}$  are the  $g_{ij}$  symmetries-decomposition coefficients while  $\varphi_{ij}^{(\gamma)}$  are the form factors listed in Tab. 2.1, a simple orthonormal rearrangement of the harmonics basis.

SC is established with a given symmetry – which means, symmetry breaking in the phase transition proceeds in a specific channel. Conventional BCS superconductivity arises from the only possible spatial structure of the local pairing,  $s$ -wave – here appearing as a local term (Fig. 2.4a)

and extended on a non-local term (Fig. 2.4b). Cuprates exhibit a tendency towards  $d_{x^2-y^2}$  SC, while other materials towards  $p$ -wave types – eventually with some chirality, as is the case for  $p_x \pm ip_y$  SCs. To establish SC under a certain symmetry  $\gamma$  means that Cooper pairs acquire said symmetry – which implies, for correlations,  $g^{(\gamma')} = g^{(\gamma)}\delta_{\gamma\gamma'}$ . and  $g_{ij} \propto \varphi_{ij}^{(\gamma)}$ .

## 2.4 Mean-Field theory reciprocal space description

In this BCS-like approach, a self-consistent equation for the gap function must be retrieved in order to further investigate the model and extract the conditions for the formation of a superconducting phase with a given pairing topology. In order to do so, let me take a step back and perform explicitly the Fourier-transform of the various terms of Eq. 1.2.

### 2.4.1 Kinetic term

The kinetic part is trivial to transform. The followed convention is

$$\hat{c}_{j\sigma} = \frac{1}{\sqrt{L_x L_y}} \sum_{\mathbf{k} \in \text{BZ}} e^{-i\mathbf{k} \cdot \mathbf{x}_j} \hat{c}_{\mathbf{k}\sigma}$$

Calculation is carried out in App. ???. Let

$$\epsilon_{\mathbf{k}} \equiv -2t [\cos(k_x \delta_x) + \cos(k_y \delta_y)]$$

then we have

$$\begin{aligned} -t \sum_{\langle ij \rangle} \sum_{\sigma} \hat{c}_{i\sigma}^\dagger \hat{c}_{j\sigma} &= \sum_{\mathbf{k}\sigma} \epsilon_{\mathbf{k}} \hat{c}_{\mathbf{k}\sigma}^\dagger \hat{c}_{\mathbf{k}\sigma} \\ &= \sum_{\mathbf{k}} \epsilon_{\mathbf{k}} \left[ \hat{c}_{\mathbf{k}\uparrow}^\dagger \hat{c}_{\mathbf{k}\uparrow} + \hat{c}_{\mathbf{k}\downarrow}^\dagger \hat{c}_{\mathbf{k}\downarrow} \right] \\ &= \sum_{\mathbf{k}} \epsilon_{\mathbf{k}} \left[ \hat{c}_{\mathbf{k}\uparrow}^\dagger \hat{c}_{\mathbf{k}\uparrow} - \hat{c}_{-\mathbf{k}\downarrow} \hat{c}_{-\mathbf{k}\downarrow}^\dagger \right] \end{aligned}$$

In last passage I used fermionic anti-commutation rules and reversed the sign of the mute variable. This will become useful later.

### 2.4.2 Non-local attraction

Consider now the result of Eq. (2.4). Taking in the mean-field approximation (with Cooper pair symmetry breaking), we get

$$\hat{c}_{\mathbf{K}+\mathbf{k}\uparrow}^\dagger \hat{c}_{\mathbf{K}-\mathbf{k}\downarrow}^\dagger \hat{c}_{\mathbf{K}-\mathbf{k}'\downarrow} \hat{c}_{\mathbf{K}+\mathbf{k}'\uparrow} \simeq \langle \hat{c}_{\mathbf{K}+\mathbf{k}\uparrow}^\dagger \hat{c}_{\mathbf{K}-\mathbf{k}\downarrow}^\dagger \rangle \hat{c}_{\mathbf{K}-\mathbf{k}'\downarrow} \hat{c}_{\mathbf{K}+\mathbf{k}'\uparrow} + \hat{c}_{\mathbf{K}+\mathbf{k}\uparrow}^\dagger \hat{c}_{\mathbf{K}-\mathbf{k}\downarrow}^\dagger \langle \hat{c}_{\mathbf{K}-\mathbf{k}'\downarrow} \hat{c}_{\mathbf{K}+\mathbf{k}'\uparrow} \rangle + \dots$$

Take e.g.  $\langle \hat{c}_{\mathbf{K}+\mathbf{k}\uparrow}^\dagger \hat{c}_{\mathbf{K}-\mathbf{k}\downarrow}^\dagger \rangle$ : the only non-zero contribution can come from the  $\mathbf{K} = \mathbf{0}$  term, as will be discussed self-consistently in Sec. 2.4.5. Then finally:

$$\hat{H}_V \simeq - \sum_{\mathbf{k}, \mathbf{k}'} V_{\mathbf{k}\mathbf{k}'} \left[ \langle \hat{\phi}_{\mathbf{k}}^\dagger \rangle \hat{\phi}_{\mathbf{k}'} + \langle \hat{\phi}_{\mathbf{k}} \rangle \hat{\phi}_{\mathbf{k}'}^\dagger \right]$$

having I defined the pairing operator

$$\hat{\phi}_{\mathbf{k}} \equiv \hat{c}_{-\mathbf{k}\downarrow} \hat{c}_{\mathbf{k}\uparrow} \quad \hat{\phi}_{\mathbf{k}}^\dagger \equiv \hat{c}_{\mathbf{k}\uparrow}^\dagger \hat{c}_{-\mathbf{k}\downarrow}^\dagger$$

and the two-body potential

$$V_{\mathbf{k}\mathbf{k}'} = \frac{2V}{L_x L_y} [\cos(\delta k_x \delta_x) + \cos(\delta k_y \delta_y)]$$

Now, consider the term

$$\cos(\delta k_x) + \cos(\delta k_y) = \cos k_x \cos k'_x + \sin k_x \sin k'_x + \cos k_y \cos k'_y + \sin k_y \sin k'_y$$

Structure	Structure factor	Graph
$s$ -wave	$\varphi_{\mathbf{k}}^{(s)} = 1$	Fig. 2.4a
Extended $s$ -wave	$\varphi_{\mathbf{k}}^{(s^*)} = \cos k_x + \cos k_y$	Fig. 2.4b
$p_x$ -wave	$\varphi_{\mathbf{k}}^{(p_x)} = i\sqrt{2} \sin k_x$	Fig. 2.4c
$p_y$ -wave	$\varphi_{\mathbf{k}}^{(p_y)} = i\sqrt{2} \sin k_y$	Fig. 2.4d
$d_{x^2-y^2}$ -wave	$\varphi_{\mathbf{k}}^{(d)} = \cos k_x - \cos k_y$	Fig. 2.4e

**Table 2.2** | Structure factors derived from the correlation structures of Tab. ???. The functions hereby defined are orthonormal, and define the various components of the non-local topological effective potential.

For the sake of readability, the notations

$$c_\ell \equiv \cos k_\ell \quad s_\ell \equiv \sin k_\ell \quad c'_\ell \equiv \cos k'_\ell \quad s'_\ell \equiv \sin k'_\ell$$

are used. Group the four terms above,

$$\underbrace{(c_x c'_x + c_y c'_y)}_{\text{Symmetric}} + \underbrace{(s_x s'_x + s_y s'_y)}_{\text{Anti-symmetric}} \quad (2.34)$$

The first two exhibit inversion symmetry for both arguments  $\mathbf{k}, \mathbf{k}'$ ; the second two exhibit anti-symmetry. Decoupling the symmetric part,

$$c_x c'_x + c_y c'_y = \frac{1}{2}(c_x + c_y)(c'_x + c'_y) + \frac{1}{2}(c_x - c_y)(c'_x - c'_y)$$

which finally gives:

$$\begin{aligned} \cos(\delta k_x) + \cos(\delta k_y) &= \frac{1}{2}(c_x + c_y)(c'_x + c'_y) && (s^*\text{-wave}) \\ &+ s_x s'_x && (p_x\text{-wave}) \\ &+ s_y s'_y && (p_y\text{-wave}) \\ &+ \frac{1}{2}(c_x - c_y)(c'_x - c'_y) && (d_{x^2-y^2}\text{-wave}) \end{aligned}$$

In other words, the two-body potential decomposes as

$$\begin{aligned} V_{\mathbf{k}\mathbf{k}'} &= \sum_{\gamma} V^{(\gamma)} \varphi_{\mathbf{k}}^{(\gamma)} \varphi_{\mathbf{k}'}^{(\gamma)*} \quad \text{where } \gamma = s^*, p_x, p_y, d_{x^2-y^2} \\ &= \frac{V}{L_x L_y} \sum_{\gamma} \varphi_{\mathbf{k}}^{(\gamma)} \varphi_{\mathbf{k}'}^{(\gamma)*} \end{aligned}$$

being  $\varphi_{\mathbf{k}}^{(\gamma)}$  the reciprocal-space expressions for the form factors of Tab. 2.1, listed explicitly in Tab. 2.2, and  $V_{\mathbf{k}\mathbf{k}'}^{(\gamma)}$  the symmetry-resolved components of the non-local attraction. Then the two-body potential has been decomposed in its planar symmetry components, each of which will naturally couple only to identically structured parameters in the full hamiltonian.

Define now the non-local gap function

$$\mathcal{V}_{\mathbf{k}} \equiv \sum_{\mathbf{k}'} V_{\mathbf{k}\mathbf{k}'} \langle \hat{\phi}_{\mathbf{k}'}^\dagger \rangle \quad (2.35)$$

one gets immediately

$$\hat{H}_V \simeq - \sum_{\mathbf{k}} \left[ \mathcal{V}_{\mathbf{k}} \hat{\phi}_{\mathbf{k}} + \mathcal{V}_{\mathbf{k}}^* \hat{\phi}_{\mathbf{k}}^\dagger \right] \quad (2.36)$$



To assume symmetry is broken in a specific symmetry channel  $\gamma$  means precisely to assume  $g_{ij} \propto \varphi_{ij}^{(\gamma)}$ , which in turn implies  $\langle \hat{\phi}_{\mathbf{k}} \rangle \propto \varphi_{\mathbf{k}}^{(\gamma)}$ . Of course, in Eq. (2.35) only the  $\gamma$  component of the potential survives, implying the gap function acquires the same symmetry,

$$\begin{aligned} \mathcal{V}_{\mathbf{k}} &\propto \sum_{\mathbf{k}'} \frac{V}{L_x L_y} \varphi_{\mathbf{k}}^{(\gamma)} \varphi_{\mathbf{k}'}^{(\gamma)*} \varphi_{\mathbf{k}'}^{(\gamma)} \\ &\propto \varphi_{\mathbf{k}}^{(\gamma)} \end{aligned}$$

where I used orthonormality of the  $\varphi_{\mathbf{k}}^{(\gamma)}$  functions.

### 2.4.3 Local interaction and gap function

A very similar argument can be carried out for the local  $U$  term. Without delving in too many details, the local gap  $\mathcal{U}_{\mathbf{k}}$  is given by

$$\mathcal{U}_{\mathbf{k}} \equiv \frac{U}{2L_x L_y} \sum_{\mathbf{k}} \langle \hat{\phi}_{\mathbf{k}} \rangle \quad (2.37)$$

evidently independent of  $\mathbf{k}$ , correctly. Identical considerations as in the above section hold for the local gap. The local part of the hamiltonian then gets

$$\hat{H}_U \simeq \sum_{\mathbf{k}} \left[ \mathcal{U}_{\mathbf{k}} \hat{\phi}_{\mathbf{k}} + \mathcal{U}_{\mathbf{k}}^* \hat{\phi}_{\mathbf{k}}^\dagger \right] \quad (2.38)$$

and the full gap function is simply

$$\Delta_{\mathbf{k}} \equiv \mathcal{V}_{\mathbf{k}} - \mathcal{U}_{\mathbf{k}} \quad (2.39)$$

Notice here that the only possible topology here is  $s$ -wave; define trivially the  $s$ -wave component of the total two-body interaction,

$$V^{(s)} = -\frac{U}{2L_x L_y}$$

Then the full effective interaction is collected in

$$\begin{aligned} \hat{H}_U + \hat{H}_V &\simeq - \sum_{\gamma} \sum_{\mathbf{k}, \mathbf{k}'} V^{(\gamma)} \varphi_{\mathbf{k}}^{(\gamma)} \varphi_{\mathbf{k}'}^{(\gamma)*} \left[ \langle \hat{\phi}_{\mathbf{k}}^\dagger \rangle \hat{\phi}_{\mathbf{k}'} + \langle \hat{\phi}_{\mathbf{k}} \rangle \hat{\phi}_{\mathbf{k}'}^\dagger \right] \\ &= - \sum_{\mathbf{k}} \left[ \Delta_{\mathbf{k}} \hat{\phi}_{\mathbf{k}} + \Delta_{\mathbf{k}}^* \hat{\phi}_{\mathbf{k}}^\dagger \right] \end{aligned}$$

The full self-consistency equation is given by

$$\Delta_{\mathbf{k}} \equiv \sum_{\mathbf{k}'} \left[ V^{(s)} + V_{\mathbf{k}\mathbf{k}'} \right] \langle \hat{\phi}_{\mathbf{k}'}^\dagger \rangle \quad (2.40)$$

The gap function decomposes in symmetry channels as well,

$$\Delta_{\mathbf{k}} = \sum_{\gamma} \Delta^{(\gamma)} \varphi_{\mathbf{k}}^{(\gamma)}$$

If SC arises in a specific symmetry channel,  $\Delta_{\mathbf{k}}$  will show the same symmetry. It follows, due to orthonormality and using Eq. (2.40),

$$\begin{aligned} \Delta^{(\gamma)} &= \frac{1}{L_x L_y} \sum_{\mathbf{k}} \varphi_{\mathbf{k}}^{(\gamma)*} \Delta_{\mathbf{k}} \\ &= \frac{1}{L_x L_y} \sum_{\mathbf{k}} \varphi_{\mathbf{k}}^{(\gamma)*} \sum_{\mathbf{k}'} \left[ V^{(s)} + V_{\mathbf{k}\mathbf{k}'} \right] \langle \hat{\phi}_{\mathbf{k}'}^\dagger \rangle \\ &= \frac{1}{L_x L_y} \sum_{\mathbf{k}} \varphi_{\mathbf{k}}^{(\gamma)*} \sum_{\mathbf{k}' \gamma'} V^{(\gamma')} \varphi_{\mathbf{k}}^{(\gamma')} \varphi_{\mathbf{k}'}^{(\gamma')*} \langle \hat{\phi}_{\mathbf{k}'}^\dagger \rangle \\ &= V^{(\gamma)} \sum_{\mathbf{k}} \varphi_{\mathbf{k}}^{(\gamma)*} \langle \hat{\phi}_{\mathbf{k}}^\dagger \rangle \end{aligned} \quad (2.41)$$

Structure	Self-consistency equation	Graph
$s$ -wave	$\Delta^{(s)} = -\frac{U}{2L_x L_y} \sum_{\mathbf{k}} \langle \hat{\phi}_{\mathbf{k}}^\dagger \rangle$	Fig. 2.4a
Extended $s$ -wave	$\Delta^{(s^*)} = \frac{V}{L_x L_y} \sum_{\mathbf{k}} (c_x + c_y) \langle \hat{\phi}_{\mathbf{k}}^\dagger \rangle$	Fig. 2.4b
$p_x$ -wave	$\Delta^{(p_x)} = -i\sqrt{2} \frac{V}{L_x L_y} \sum_{\mathbf{k}} s_x \langle \hat{\phi}_{\mathbf{k}}^\dagger \rangle$	Fig. 2.4c
$p_y$ -wave	$\Delta^{(p_y)} = -i\sqrt{2} \frac{V}{L_x L_y} \sum_{\mathbf{k}} s_y \langle \hat{\phi}_{\mathbf{k}}^\dagger \rangle$	Fig. 2.4d
$d_{x^2-y^2}$ -wave	$\Delta^{(d)} = \frac{V}{L_x L_y} \sum_{\mathbf{k}} (c_x - c_y) \langle \hat{\phi}_{\mathbf{k}}^\dagger \rangle$	Fig. 2.4e

**Table 2.3** Symmetry resolved self-consistency equations for the MFT parameters  $\Delta^{(\gamma)}$ , based on Eq. (2.40) and (2.41). By computing  $\langle \hat{\phi}_{\mathbf{k}}^\dagger \rangle$ , it is possible to reconstruct the various components of the gap function.

This result provides a set of self-consistency equations for each symmetry channel, listed in Tab. 2.3. Notice that to reconstruct self-consistently the full  $s$ -wave phase transition, the actual gap function is given by

$$\Delta^{(s)} + \Delta^{(s^*)}(c_x + c_y)$$

The  $s$ -wave transition is the only one equipped of both the local and the non-local parts. Within this structure, we are finally able to move to Nambu formalism.

#### 2.4.4 Nambu formalism and Bogoliubov transform

Define the Nambu spinor<sup>2</sup> as in BCS

$$\hat{\Psi}_{\mathbf{k}} \equiv \begin{bmatrix} \hat{c}_{\mathbf{k}\uparrow} \\ \hat{c}_{-\mathbf{k}\downarrow}^\dagger \end{bmatrix}$$

Evidently,

$$\phi_{\mathbf{k}} = \hat{\Psi}_{\mathbf{k}}^\dagger \begin{bmatrix} 0 & 1 \\ 0 & 0 \end{bmatrix} \hat{\Psi}_{\mathbf{k}} \quad \phi_{\mathbf{k}}^\dagger = \hat{\Psi}_{\mathbf{k}}^\dagger \begin{bmatrix} 0 & 0 \\ 1 & 0 \end{bmatrix} \hat{\Psi}_{\mathbf{k}} \quad (2.42)$$

The full hamiltonian is then given by:

$$\hat{H} = \sum_{\mathbf{k}} \hat{\Psi}_{\mathbf{k}} h_{\mathbf{k}} \hat{\Psi}_{\mathbf{k}} \quad h_{\mathbf{k}} \equiv \begin{bmatrix} \epsilon_{\mathbf{k}} & -\Delta_{\mathbf{k}}^* \\ -\Delta_{\mathbf{k}} & -\epsilon_{\mathbf{k}} \end{bmatrix} \quad (2.43)$$

Let  $\tau^\alpha$  for  $\alpha = x, y, z$  be the Pauli matrices. Define:

$$\hat{s}_{\mathbf{k}}^\alpha \equiv \hat{\Psi}_{\mathbf{k}}^\dagger \tau^\alpha \hat{\Psi}_{\mathbf{k}} \quad \text{for } \alpha = x, y, z$$

As can be shown easily, these operators realize spin-1/2 algebra.  $\hat{H}$  represents an ensemble of  $L_x L_y$  independent spins subject to pseudo-magnetic fields. Note that, differently from App. ?? where the chemical potential is inserted later (because in Nambu formalism it accounts for a diagonal term) here the chemical potential is part of the  $z$  component of the pseudo-magnetic field, since

$$\begin{aligned} \hat{n}_{\mathbf{k}\uparrow} + \hat{n}_{-\mathbf{k}\downarrow} &= \hat{c}_{\mathbf{k}\uparrow}^\dagger \hat{c}_{\mathbf{k}\uparrow} + \hat{c}_{-\mathbf{k}\downarrow}^\dagger \hat{c}_{-\mathbf{k}\downarrow} \\ &= \hat{c}_{\mathbf{k}\uparrow}^\dagger \hat{c}_{\mathbf{k}\uparrow} - \hat{c}_{-\mathbf{k}\downarrow} \hat{c}_{-\mathbf{k}\downarrow}^\dagger + \mathbb{I} \\ &= \hat{\Psi}_{\mathbf{k}}^\dagger \tau^z \hat{\Psi}_{\mathbf{k}} + \mathbb{I} \end{aligned} \quad (2.44)$$

<sup>2</sup>Notice that the spinor is here differently defined with respect to App. 4, where because of the HF prevalence in mean-field decoupling the spinor components were homogeneously fermions creations or destructions.

and then it follows

$$\begin{aligned} -\mu\hat{N} &= -\mu \sum_{\mathbf{k} \in \text{BZ}} [\hat{n}_{\mathbf{k}\uparrow} + \hat{n}_{-\mathbf{k}\downarrow}] \\ &= -\mu \sum_{\mathbf{k} \in \text{BZ}} \hat{\Psi}_{\mathbf{k}}^\dagger \tau^z \hat{\Psi}_{\mathbf{k}} - \mu L_x L_y \end{aligned}$$

Then, adding a term  $-\mu\hat{N}$  to  $\hat{H}$ , apart from an irrelevant total energy increase, changes the pseudo-field whose explicit form becomes

$$\mathbf{b}_{\mathbf{k}} \equiv \begin{bmatrix} -\text{Re}\{\Delta_{\mathbf{k}}\} \\ -\text{Im}\{\Delta_{\mathbf{k}}\} \\ \epsilon_{\mathbf{k}} - \mu \end{bmatrix} \quad (2.45)$$

This hamiltonian behaves as an ensemble of spins in local magnetic fields precisely as in Eq. (4.5),

$$\hat{H} - \mu\hat{N} = \sum_{\mathbf{k} \in \text{BZ}} \mathbf{b}_{\mathbf{k}} \cdot \hat{\mathbf{s}}_{\mathbf{k}} \quad \text{where} \quad \hat{\mathbf{s}}_{\mathbf{k}\sigma} = \begin{bmatrix} \hat{s}_{\mathbf{k}}^x \\ \hat{s}_{\mathbf{k}}^y \\ \hat{s}_{\mathbf{k}}^z \end{bmatrix} \quad (2.46)$$

Proceed as in App. ?? and diagonalize via a rotation,

$$d_{\mathbf{k}} \equiv \begin{bmatrix} -E_{\mathbf{k}} & \\ & E_{\mathbf{k}} \end{bmatrix} \quad \text{being} \quad E_{\mathbf{k}} \equiv \sqrt{\xi_{\mathbf{k}}^2 + |\Delta_{\mathbf{k}}|^2}$$

and  $\xi_{\mathbf{k}} \equiv \epsilon_{\mathbf{k}} - \mu$ . Given the pseudoangles

$$\tan(2\theta_{\mathbf{k}}) \equiv \frac{|\Delta_{\mathbf{k}}|}{\epsilon_{\mathbf{k}}} \quad \tan(2\zeta_{\mathbf{k}}) \equiv \frac{\text{Im}\{\Delta_{\mathbf{k}}\}}{\text{Re}\{\Delta_{\mathbf{k}}\}}$$

the general diagonalizer will be an orthogonal rotation matrix

$$\begin{aligned} W_{\mathbf{k}} &= e^{i(\theta_{\mathbf{k}} - \frac{\pi}{2})\tau^y} e^{i\zeta_{\mathbf{k}}\tau^z} \\ &= \begin{bmatrix} -\sin\theta_{\mathbf{k}} & -\cos\theta_{\mathbf{k}} \\ \cos\theta_{\mathbf{k}} & -\sin\theta_{\mathbf{k}} \end{bmatrix} \begin{bmatrix} e^{i\zeta_{\mathbf{k}}} & \\ & e^{-i\zeta_{\mathbf{k}}} \end{bmatrix} \\ &= \begin{bmatrix} -\sin\theta_{\mathbf{k}}e^{i\zeta_{\mathbf{k}}} & -\cos\theta_{\mathbf{k}}e^{-i\zeta_{\mathbf{k}}} \\ \cos\theta_{\mathbf{k}}e^{i\zeta_{\mathbf{k}}} & -\sin\theta_{\mathbf{k}}e^{-i\zeta_{\mathbf{k}}} \end{bmatrix} \end{aligned} \quad (2.47)$$

given by a rotation of angle  $\zeta_{\mathbf{k}}$  around the  $z$  axis, to align the  $x$  axis with the field projection onto the  $xy$  plane, followed by a rotation around the  $y$  axis to anti-align with the pseudo-field. The MFT-BCS solution is given by a degenerate Fermi gas at ground state, whose quasi-particles occupy two bands  $\pm E_{\mathbf{k}}$  and their fermionic operators are given by

$$\hat{\gamma}_{\mathbf{k}}^{(-)} \equiv [W_{\mathbf{k}}\hat{\Psi}_{\mathbf{k}}]_1 \quad \hat{\gamma}_{\mathbf{k}}^{(+)} \equiv [W_{\mathbf{k}}\hat{\Psi}_{\mathbf{k}}]_2$$

The diagonalization operators are given by

$$\hat{\Gamma}_{\mathbf{k}} \equiv W_{\mathbf{k}}\hat{\Psi}_{\mathbf{k}} \quad \text{where} \quad \hat{\Gamma}_{\mathbf{k}} = \begin{bmatrix} \hat{\gamma}_{\mathbf{k}}^{(-)} \\ \hat{\gamma}_{\mathbf{k}}^{(+)} \end{bmatrix}$$

then, using Eq. (4.12),

$$\langle [\hat{\Psi}_{\mathbf{k}}^\dagger]_i [\hat{\Psi}_{\mathbf{k}}]_j \rangle = [W_{\mathbf{k}}]_{1i} [W_{\mathbf{k}}^\dagger]_{j1} f(-E_{\mathbf{k}}; \beta, 0) + [W_{\mathbf{k}}]_{2i} [W_{\mathbf{k}}^\dagger]_{j2} f(E_{\mathbf{k}}; \beta, 0)$$

where in the Fermi-Dirac function chemical potential was set to zero, because it already was included in the diagonalized hamiltonian. Recalling Eq. (??), it follows

$$\langle \phi_{\mathbf{k}}^\dagger \rangle = [W_{\mathbf{k}}]_{11} [W_{\mathbf{k}}^\dagger]_{21} f(-E_{\mathbf{k}}; \beta, 0) + [W_{\mathbf{k}}]_{21} [W_{\mathbf{k}}^\dagger]_{22} f(E_{\mathbf{k}}; \beta, 0) \quad (2.48)$$

$$= \frac{1}{2} \sin(2\theta_{\mathbf{k}}) e^{i2\zeta_{\mathbf{k}}} \tanh\left(\frac{\beta E_{\mathbf{k}}}{2}\right) \quad (2.49)$$

The last passage has been obtained by computing the matrix element from the explicit form of  $W_{\mathbf{k}}$  of Eq. (2.47) and by the simple relation

$$\begin{aligned} \frac{1}{e^{-x} + 1} - \frac{1}{e^x + 1} &= \frac{e^x - 1}{e^x + 1} \\ &= \tanh\left(\frac{x}{2}\right) \end{aligned}$$

Eqs. (2.48), (2.49) give us both the algorithmic formula (first row) and its theoretical counterpart (second row) to compute the order parameters in the HF approach at each point in  $k$ -space ( $k_x, k_y$ ). We can finally derive the BCS self-consistency equation

$$\Delta_{\mathbf{k}} \equiv \frac{1}{2} \sum_{\mathbf{k}'} \left[ V^{(s)} + V_{\mathbf{k}\mathbf{k}'} \right] \frac{|\Delta_{\mathbf{k}}|}{\sqrt{\xi_{\mathbf{k}}^2 + |\Delta_{\mathbf{k}}|^2}} e^{i \operatorname{Im}\{\Delta_{\mathbf{k}}\} / \operatorname{Re}\{\Delta_{\mathbf{k}}\}} \tanh\left(\frac{\beta}{2} \sqrt{\xi_{\mathbf{k}}^2 + |\Delta_{\mathbf{k}}|^2}\right) \quad (2.50)$$

The whole point of the HF algorithm is to find an iterative solution for each symmetry channel, using the self-consistency equation projection of Tab. 2.3.

Notice that the  $z$  component of the spin operators is related to density: using Eq. (4.12),

$$\langle \hat{\Psi}_{\mathbf{k}}^\dagger \tau^z \hat{\Psi}_{\mathbf{k}} \rangle = \langle [\hat{\Psi}_{\mathbf{k}}^\dagger]_1 [\hat{\Psi}_{\mathbf{k}}]_1 \rangle - \langle [\hat{\Psi}_{\mathbf{k}}^\dagger]_2 [\hat{\Psi}_{\mathbf{k}}]_2 \rangle$$

I proceed in as done previously, and from Eq. (2.44),

$$\begin{aligned} \langle \hat{n}_{\mathbf{k}\uparrow} \rangle + \langle \hat{n}_{-\mathbf{k}\downarrow} \rangle &= 1 + \langle \hat{\Psi}_{\mathbf{k}}^\dagger \tau^z \hat{\Psi}_{\mathbf{k}} \rangle \\ &= 1 + \left( |[W_{\mathbf{k}}]_{11}|^2 - |[W_{\mathbf{k}}]_{12}|^2 \right) f(-E_{\mathbf{k}}; \beta, 0) \\ &\quad + \left( |[W_{\mathbf{k}}]_{21}|^2 - |[W_{\mathbf{k}}]_{22}|^2 \right) f(E_{\mathbf{k}}; \beta, 0) \end{aligned} \quad (2.51)$$

$$= 1 - \cos(2\theta_{\mathbf{k}}) \tanh\left(\frac{\beta E_{\mathbf{k}}}{2}\right) \quad (2.52)$$

The expectation value for the density is needed in order to extract the optimal chemical potential  $\mu$  for the target density we aim to simulate at the given parametrization. This is numerically obtained by using Eq. (2.51) directly on the diagonalization matrix of  $h_{\mathbf{k}}$ .

#### 2.4.5 A short comment on self-consistency

The Bogoliubov fermions in spinor representation satisfy obviously  $\hat{\Psi}_{\mathbf{k}} = W_{\mathbf{k}}^\dagger \hat{\Gamma}_{\mathbf{k}}$ . Consider e.g.

$$\langle \hat{c}_{\mathbf{k}\sigma}^\dagger \hat{c}_{-\mathbf{k}\sigma}^\dagger \rangle$$

which is a spin-symmetric anomalous Cooper pair. For simplicity, take  $\sigma = \uparrow$ . Expand:

$$\begin{aligned} \langle \hat{c}_{\mathbf{k}\uparrow}^\dagger \hat{c}_{-\mathbf{k}\uparrow}^\dagger \rangle &= \langle [\hat{\Psi}_{\mathbf{k}}^\dagger]_1 [\hat{\Psi}_{-\mathbf{k}}^\dagger]_1 \rangle \\ &= \langle [W_{\mathbf{k}} \hat{\Gamma}_{\mathbf{k}}^\dagger]_1 [W_{-\mathbf{k}} \hat{\Gamma}_{-\mathbf{k}}^\dagger]_1 \rangle \end{aligned}$$

This expectation value is taken over the ground-state, the latter being the vacuum of  $\Gamma$  fermions. Evidently the above expectation cannot assume non-zero values. Obviously the same holds for  $\sigma = \downarrow$ , and this argument explains why the Ferromagnetic terms of the hamiltonian decomposition do not contribute to Cooper instability. An identical argument, with the exchange

$$(\sigma, \sigma) \rightarrow (\uparrow, \downarrow) \quad \text{and} \quad (\mathbf{k}, -\mathbf{k}) \rightarrow (\mathbf{K} + \mathbf{k}, \mathbf{K} - \mathbf{k}) \quad \text{with} \quad \mathbf{K} \neq \mathbf{0}$$

justifies why in Sec. 2.4.4 the only relevant contribution was given by  $\mathbf{K} = \mathbf{0}$ . In the next sections, the results of the self-consistent HF algorithm are exposed.

## 2.5 Results of the HF algorithm

[To be continued...]

## Chapter 3

# Superexchange and virtual hopping in Hubbard lattices

A key mechanism in AF phase formation in Hubbard lattice is superexchange. The AF phase is stabilized by spin fluctuations and second-order virtual hopping. The mechanism becomes clear enough by considering a 2-sites Hubbard toy model.

### 3.1 Virtual hopping in the 2-sites Hubbard lattice

Consider the toy model:

$$\hat{H} = -t \left\{ \hat{c}_{1\uparrow}^\dagger \hat{c}_{2\uparrow} + \hat{c}_{1\downarrow}^\dagger \hat{c}_{2\downarrow} + \text{h.c.} \right\} + U \{ \hat{n}_{1\uparrow} \hat{n}_{1\downarrow} + \hat{n}_{2\uparrow} \hat{n}_{2\downarrow} \}$$

with  $i = 1, 2$  the site index. The two sites are represented in Fig. 3.1. The two competing processes are:

1. electrons inter-sites hopping with amplitude  $-t$ ;
2. local repulsion  $+U$ , acting when two anti-aligned electrons reside on the same site;

For an half-filled system, the Hilbert space is six-dimensional. I use the notation  $|n_{1\uparrow} n_{1\downarrow} n_{2\uparrow} n_{2\downarrow}\rangle$  to indicate the six computational basis states:

$$\begin{array}{lll} |\psi_1\rangle \equiv |1010\rangle & |\psi_3\rangle \equiv |1001\rangle & |\psi_5\rangle \equiv |0011\rangle \\ |\psi_2\rangle \equiv |1100\rangle & |\psi_4\rangle \equiv |0110\rangle & |\psi_6\rangle \equiv |0101\rangle \end{array}$$

For example, the top panel of Fig. 3.1 shows state  $|\psi_2\rangle$ .

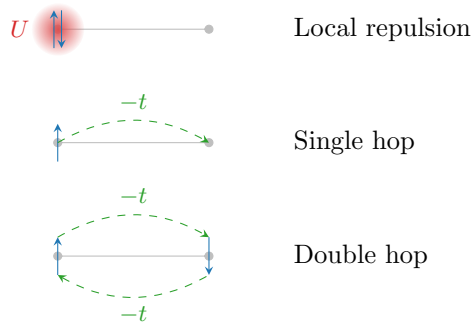


Figure 3.1 | Two sites Hubbard model.

Structure	Eigenstate	Energy
Spin-1/2 singlet	$\frac{ \phi_3\rangle -  \phi_4\rangle}{\sqrt{2}}$	$E^- = \frac{U}{2} - \sqrt{\frac{U^2}{4} + 4t^2}$
Spin-1/2 triplet	$ \phi_1\rangle, \frac{ \phi_3\rangle +  \phi_4\rangle}{\sqrt{2}},  \phi_6\rangle$	0
	$\frac{ \phi_2\rangle -  \phi_5\rangle}{\sqrt{2}}$	$U$
	$\frac{ \phi_2\rangle +  \phi_5\rangle}{\sqrt{2}}$	$E^+ = \frac{U}{2} + \sqrt{\frac{U^2}{4} + 4t^2}$

**Table 3.1** | List of exact eigenstates and relative energies for the 2-sites half-filled Hubbard model.

### 3.1.1 Exact solution of the half-filled model

The hamiltonian matrix is directly evaluated in this basis

$$H_{ij} = \langle \psi_i | \hat{H} | \psi_j \rangle \implies H = \begin{bmatrix} 0 & & & & & \\ & U & -t & -t & & \\ & -t & & & -t & \\ & -t & & & -t & \\ & & -t & -t & U & \\ & & & & & 0 \end{bmatrix}$$

Empty slots in the matrix stand for zeros. Evidently the states  $|\psi_1\rangle$  (both up) and  $|\psi_6\rangle$  (both down) are zero-energy eigenstates. These states cannot realize electrons hopping because of Pauli principle. The internal  $4 \times 4$  matrix is readily diagonalized by the means of a change of basis  $V$ ,

$$V \begin{bmatrix} U & -t & -t & \\ -t & & & -t \\ -t & & & -t \\ & -t & -t & U \end{bmatrix} V^\dagger = \begin{bmatrix} E^- & & & \\ & 0 & & \\ & & U & \\ & & & E^+ \end{bmatrix}$$

Tab. 3.1 shows the eigenvectors and relative eigenvalues obtained from diagonalization. The ground-state is the singlet state,

$$\frac{|\phi_3\rangle - |\phi_4\rangle}{\sqrt{2}} = \frac{|1010\rangle - |0101\rangle}{\sqrt{2}} = \frac{|\uparrow\downarrow\rangle - |\downarrow\uparrow\rangle}{\sqrt{2}}$$

of energy

$$E^- = \frac{U}{2} - \sqrt{\frac{U^2}{4} + 4t^2} \simeq -\frac{4t^2}{U}$$

the latter equality being true if  $U \gg t$  (strong repulsion limit). The singlet state pairs with a spatially-symmetric (nodeless) wavefunction. The entire triplet (second row of Tab. 3.1) remains at zero energy. Excited states are anti-symmetrized and symmetrized version of the polarized states  $|\phi_1\rangle$  and  $|\phi_6\rangle$ .

### 3.1.2 Virtual hopping

The key feature of the singlet state is the one represented in the bottom panel of Fig. 3.1: if the two electrons occupy separate sites and are anti-aligned, both “see” the other site as empty, thus free to hop to. [To be continued...]

## Chapter 4

# Mean-Field Theory in Hubbard lattices

In this Appendix the Mean-Field solutions to the Hubbard hamiltonian,

$$\hat{H} = -t \sum_{\langle ij \rangle} \sum_{\sigma} \hat{c}_{i\sigma}^{\dagger} \hat{c}_{j\sigma} + U \sum_i \hat{n}_{i\uparrow} \hat{n}_{i\downarrow} \quad t, U > 0$$

are described. The discussion is limited to the two-dimensional square lattice. The two-dimensional square lattice extension of the two-sites model can be studied by the means of Mean Field Theory. We have:

$$\begin{aligned} \hat{n}_{i\uparrow} \hat{n}_{i\downarrow} &= (\langle \hat{n}_{i\uparrow} \rangle + \delta \hat{n}_{i\uparrow}) (\langle \hat{n}_{i\downarrow} \rangle + \delta \hat{n}_{i\downarrow}) \\ &\simeq \langle \hat{n}_{i\uparrow} \rangle \langle \hat{n}_{i\downarrow} \rangle + \delta \hat{n}_{i\uparrow} \langle \hat{n}_{i\downarrow} \rangle + \langle \hat{n}_{i\uparrow} \rangle \delta \hat{n}_{i\downarrow} + \mathcal{O}(\delta n^2) \\ &= -\langle \hat{n}_{i\uparrow} \rangle \langle \hat{n}_{i\downarrow} \rangle + \hat{n}_{i\uparrow} \langle \hat{n}_{i\downarrow} \rangle + \langle \hat{n}_{i\uparrow} \rangle \hat{n}_{i\downarrow} + \mathcal{O}(\delta n^2) \end{aligned}$$

where  $\delta \hat{n}_{i\sigma} \equiv \hat{n}_{i\sigma} - \langle \hat{n}_{i\sigma} \rangle$  and orders higher than first have been ignored, assuming negligible fluctuations around the equilibrium single-site population. The first term of the above three can be neglected at fixed particles number, being a pure energy shift.

### 4.1 Ferromagnetic solution

The Mean-Field Theory ferromagnetic solution prescribes an uniformly magnetized lattice,

$$\langle \hat{n}_{i\uparrow} \rangle = n + m \quad \langle \hat{n}_{i\downarrow} \rangle = n - m$$

where  $n$  is the site electron density and  $m$  is the density unbalance, leading to a magnetization per site  $2m$ . The mean-field hamiltonian with these substitutions becomes:

$$\begin{aligned} \hat{H} &\simeq -t \sum_{\langle ij \rangle} \sum_{\sigma} \hat{c}_{i\sigma}^{\dagger} \hat{c}_{j\sigma} + U \sum_i [\hat{n}_{i\uparrow} \langle \hat{n}_{i\downarrow} \rangle + \langle \hat{n}_{i\uparrow} \rangle \hat{n}_{i\downarrow}] \\ &= -t \sum_{\langle ij \rangle} \sum_{\sigma} \hat{c}_{i\sigma}^{\dagger} \hat{c}_{j\sigma} + nU \sum_i [\hat{n}_{i\uparrow} + \hat{n}_{i\downarrow}] - mU \sum_i [\hat{n}_{i\uparrow} - \hat{n}_{i\downarrow}] \end{aligned}$$

Fourier transforming,

$$\begin{aligned} -t \sum_{\langle ij \rangle} \sum_{\sigma} \hat{c}_{i\sigma}^{\dagger} \hat{c}_{j\sigma} &= -2t \sum_{\mathbf{k}\sigma} [\cos(k_x) + \cos(k_y)] \hat{n}_{\mathbf{k}\sigma} \\ nU \sum_i [\hat{n}_{i\uparrow} + \hat{n}_{i\downarrow}] &= nU \sum_{\mathbf{k}\sigma} \hat{n}_{\mathbf{k}\sigma} \\ mU \sum_i [\hat{n}_{i\uparrow} - \hat{n}_{i\downarrow}] &= mU \sum_{\mathbf{k}\sigma} [\hat{n}_{\mathbf{k}\uparrow} - \hat{n}_{\mathbf{k}\downarrow}] \end{aligned}$$

having used adimensional lattice momenta. For a square lattice, the Brillouin Zone is delimited by

$$\mathbf{k} \in [-\pi, \pi] \times [-\pi, \pi]$$

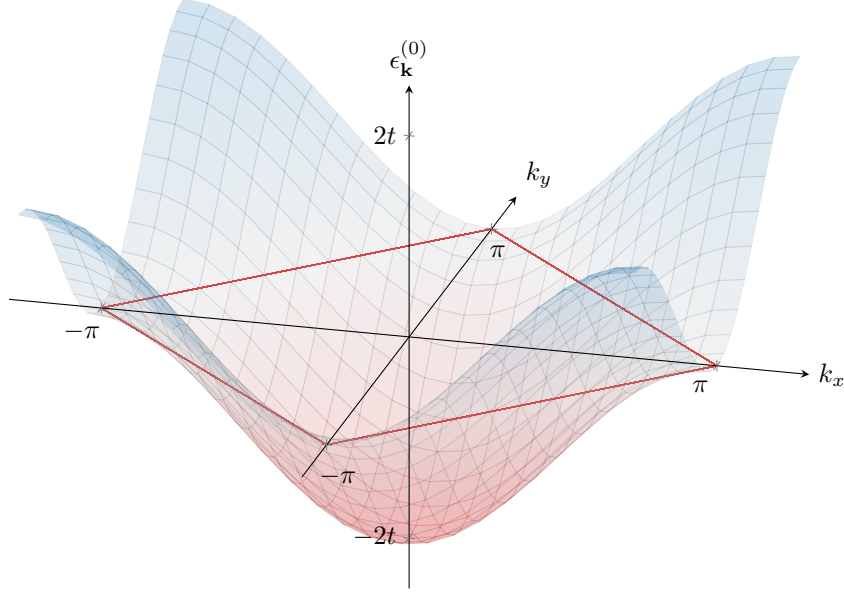


**Figure 4.1** | Depiction of the Hubbard square lattice hopping band  $\epsilon_{\mathbf{k}}^{(0)} = -2t[\cos(k_x) + \cos(k_y)]$ . The red lines mark the zero-energy intersection.

The hopping single-state energy is given by

$$\epsilon_{\mathbf{k}}^{(0)} = -2t [\cos(k_x) + \cos(k_y)]$$

represented as a band in Fig. 4.1. At  $U = 0$ , the mean-field ferromagnetic state fills the band bottom-up. The single-state energy becomes:

$$\begin{aligned} \epsilon_{\mathbf{k}\uparrow} &= U(n - m) - 2t [\cos(k_x) + \cos(k_y)] \\ \epsilon_{\mathbf{k}\downarrow} &= U(n + m) - 2t [\cos(k_x) + \cos(k_y)] \end{aligned}$$

Now it is a matter of finding the optimal value for  $m$ , minimizing the total energy at fixed filling  $\rho = 2n$ . Notice that said minimization is performed parametrically varying the magnetization  $m$ , inside the ferromagnetic-polarized space. As it turns out, for strong local repulsion  $U/t \gg 1$ , antiferromagnetic ordering is preferred. Comparison is needed in order to assess which magnetic ordering is preferred.

Consider the half-filling situation. An unpolarized system will have  $n = 1/4$ ,  $m = 0$ : this implies  $\langle \hat{n}_{i\uparrow} \rangle = \langle \hat{n}_{i\downarrow} \rangle = 1/4$ . A perfectly up-ferromagnetic system,  $n = 1/4$ ,  $m = 1/4$ : then  $\langle \hat{n}_{i\uparrow} \rangle = 1/2$  and  $\langle \hat{n}_{i\downarrow} \rangle = 0$ . [To be continued...]

## 4.2 Antiferromagnetic solution

Consider now an AF mean-field solution. Let me change notation for a brief moment, indicating each site as

$$i \rightarrow \mathbf{r} = (x, y) \quad x, y \in \mathbb{N}$$

The mean-field AF solution at half-filling is the uniform-modulated magnetization

$$m_{\mathbf{r}} = (-1)^{x+y} m \quad m \in [-1, 1]$$

and a mean-field Ansatz

$$\langle \hat{n}_{\mathbf{r}\uparrow} \rangle = n + m_{\mathbf{r}} \quad \langle \hat{n}_{\mathbf{r}\downarrow} \rangle = n - m_{\mathbf{r}} \quad (4.1)$$

With respect to the solution presented above, the only detail changing is the last term,

$$\hat{H} = -t \sum_{\langle \mathbf{r}\mathbf{r}' \rangle} \sum_{\sigma} \hat{c}_{\mathbf{r}\sigma}^{\dagger} \hat{c}_{\mathbf{r}'\sigma} + nU \sum_{\mathbf{r}} [\hat{n}_{\mathbf{r}\uparrow} + \hat{n}_{\mathbf{r}\downarrow}] - mU \sum_{\mathbf{r}} (-1)^{x+y} [\hat{n}_{\mathbf{r}\uparrow} - \hat{n}_{\mathbf{r}\downarrow}] \quad (4.2)$$



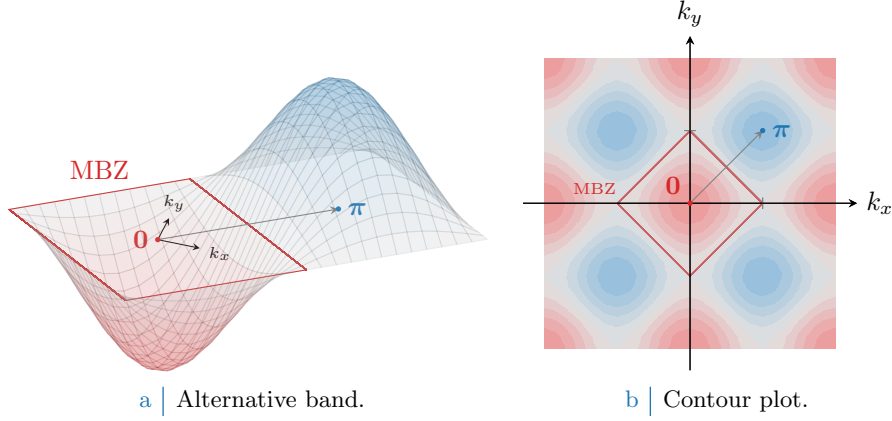


**Figure 4.2** | Alternative depiction of the Hubbard square lattice hopping band previously reported in Fig. 4.1. The Magnetic Brillouin Zone (MBZ) is delimited by the zero-energy contour and is indicated in figure. As it is evident, energy sign flips by taking a  $(\pi, \pi)$  translation in  $\mathbf{k}$  space.

Fourier-transforming, the phase factor can be absorbed in the destruction operator inside of  $\hat{n}_{\mathbf{r}\sigma}$ :

$$\begin{aligned}
 \sum_{\mathbf{r}} (-1)^{x+y} \hat{n}_{\mathbf{r}\sigma} &= \sum_{\mathbf{r}} (-1)^{x+y} \hat{c}_{\mathbf{r}\sigma}^\dagger \hat{c}_{\mathbf{r}\sigma} \\
 &= \sum_{\mathbf{r}} e^{i\pi \cdot \mathbf{r}} \frac{1}{L} \sum_{\mathbf{k} \in \text{BZ}} e^{i\mathbf{k} \cdot \mathbf{r}} \hat{c}_{\mathbf{k}\sigma}^\dagger \frac{1}{L} \sum_{\mathbf{k}' \in \text{BZ}} e^{-i\mathbf{k}' \cdot \mathbf{r}} \hat{c}_{\mathbf{k}'\sigma} \\
 &= \sum_{\mathbf{k} \in \text{BZ}} \sum_{\mathbf{k}' \in \text{BZ}} \hat{c}_{\mathbf{k}\sigma}^\dagger \hat{c}_{\mathbf{k}'\sigma} \frac{1}{L^2} \sum_{\mathbf{r}} e^{-i[\mathbf{k}' - (\mathbf{k} + \boldsymbol{\pi})] \cdot \mathbf{r}} \\
 &= \sum_{\mathbf{k} \in \text{BZ}} \hat{c}_{\mathbf{k}\sigma}^\dagger \hat{c}_{\mathbf{k} + \boldsymbol{\pi}\sigma}
 \end{aligned}$$

where  $\boldsymbol{\pi} = (\pi, \pi)$ . It follows:

$$mU \sum_{\mathbf{r}} (-1)^{x+y} [\hat{n}_{\mathbf{r}\uparrow} - \hat{n}_{\mathbf{r}\downarrow}] = \Delta \sum_{\mathbf{k} \in \text{BZ}} \left[ \hat{c}_{\mathbf{k}\uparrow}^\dagger \hat{c}_{\mathbf{k} + \boldsymbol{\pi}\uparrow} - \hat{c}_{\mathbf{k}\downarrow}^\dagger \hat{c}_{\mathbf{k} + \boldsymbol{\pi}\downarrow} \right] \quad \text{where} \quad \Delta \equiv mU$$

Consider the band of Fig. 4.1 at half-filling. As does Fabrizio [3], the area delimited externally by the solid lines at zero energy is denominated “Magnetic Brillouin Zone” (MBZ). The periodicity of  $\mathbf{k}$  space guarantees that the full BZ can be taken as well to be the one of Fig. 4.2a. Then:

$$\begin{aligned}
 \sum_{\mathbf{k} \in \text{BZ}} \hat{c}_{\mathbf{k}\uparrow}^\dagger \hat{c}_{\mathbf{k} + \boldsymbol{\pi}\uparrow} &= \sum_{\mathbf{k} \in \text{MBZ}} \left[ \hat{c}_{\mathbf{k}\uparrow}^\dagger \hat{c}_{\mathbf{k} + \boldsymbol{\pi}\uparrow} + \hat{c}_{\mathbf{k} + \boldsymbol{\pi}\uparrow}^\dagger \hat{c}_{\mathbf{k} + 2\boldsymbol{\pi}\uparrow} \right] \\
 &= \sum_{\mathbf{k} \in \text{MBZ}} \left[ \hat{c}_{\mathbf{k}\uparrow}^\dagger \hat{c}_{\mathbf{k} + \boldsymbol{\pi}\uparrow} + \hat{c}_{\mathbf{k} + \boldsymbol{\pi}\uparrow}^\dagger \hat{c}_{\mathbf{k}\uparrow} \right]
 \end{aligned} \tag{4.3}$$

and the same applies for spin  $\downarrow$ . Periodicity by shifts  $2\boldsymbol{\pi}$  has been used. Now, define the Nambu spinors:

$$\hat{\Psi}_{\mathbf{k}\sigma} \equiv \begin{bmatrix} \hat{c}_{\mathbf{k}\sigma} \\ \hat{c}_{\mathbf{k} + \boldsymbol{\pi}\sigma} \end{bmatrix}$$

and a spin-wise gap,

$$\Delta_{\uparrow} = \Delta \quad \Delta_{\downarrow} = -\Delta$$

At fixed filling, the  $U$  term is a pure energy shift, thus will be neglected. The kinetic term

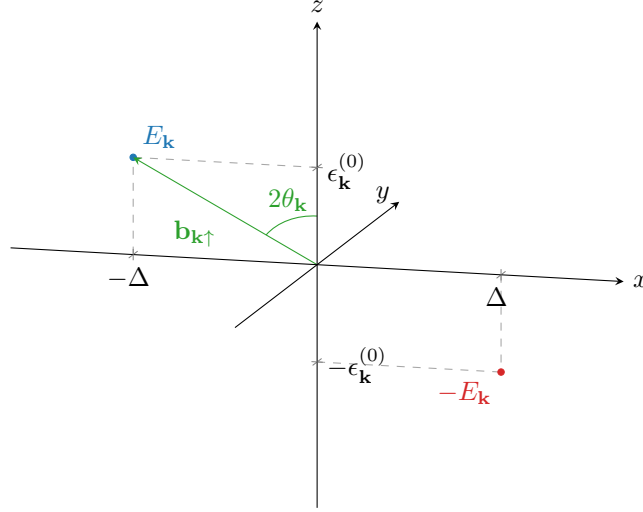


Figure 4.3 | Pseudo-magnetic field originating from mean-field treatment of the square Hubbard hamiltonian. Here, only the  $\sigma = \uparrow$

transforms as

$$\begin{aligned}
 -t \sum_{\langle ij \rangle} \sum_{\sigma} \hat{c}_{i\sigma}^{\dagger} \hat{c}_{j\sigma} &= \sum_{\mathbf{k} \in \text{BZ}} \sum_{\sigma} \epsilon_{\mathbf{k}}^{(0)} \hat{c}_{\mathbf{k}\sigma}^{\dagger} \hat{c}_{\mathbf{k}\sigma} \\
 &= \sum_{\mathbf{k} \in \text{MBZ}} \sum_{\sigma} \left[ \epsilon_{\mathbf{k}}^{(0)} \hat{c}_{\mathbf{k}\sigma}^{\dagger} \hat{c}_{\mathbf{k}\sigma} + \epsilon_{\mathbf{k}+\boldsymbol{\pi}}^{(0)} \hat{c}_{\mathbf{k}+\boldsymbol{\pi}\sigma}^{\dagger} \hat{c}_{\mathbf{k}+\boldsymbol{\pi}\sigma} \right] \\
 &= \sum_{\mathbf{k} \in \text{MBZ}} \sum_{\sigma} \epsilon_{\mathbf{k}}^{(0)} \left[ \hat{c}_{\mathbf{k}\sigma}^{\dagger} \hat{c}_{\mathbf{k}\sigma} - \hat{c}_{\mathbf{k}+\boldsymbol{\pi}\sigma}^{\dagger} \hat{c}_{\mathbf{k}+\boldsymbol{\pi}\sigma} \right]
 \end{aligned}$$

In the second passage, the sum over the full BZ was written considering that the entirety of the zone is given by all the points in the MBZ plus their conjugates obtained by a  $\boldsymbol{\pi}$  shift in the flipped band. As depicted in Fig. 4.2a, kinetic energy is anti-periodic in  $\mathbf{k}$  space by a vector  $\boldsymbol{\pi}$ . This anti-periodicity accounts for the minus sign arising in the third passage. The hamiltonian is then given by:

$$\hat{H} = \sum_{\mathbf{k} \in \text{MBZ}} \sum_{\sigma} \hat{\Psi}_{\mathbf{k}\sigma}^{\dagger} h_{\mathbf{k}\sigma} \hat{\Psi}_{\mathbf{k}\sigma} \quad \text{being} \quad h_{\mathbf{k}\sigma} \equiv \begin{bmatrix} \epsilon_{\mathbf{k}}^{(0)} & -\Delta_{\sigma} \\ -\Delta_{\sigma} & -\epsilon_{\mathbf{k}}^{(0)} \end{bmatrix} \quad (4.4)$$

Notice: the Nambu hamiltonian is a  $2 \times 2$  matrix over the MBZ – which is half the full BZ, coherently with a solution which essentially bipartites the lattice giving back a double sized unit cell.

The system ground-state is obtained by the means of a Bogoliubov rotation. The hamiltonian maps onto the simple one of a spin in a magnetic field,

$$h_{\mathbf{k}\sigma} = \epsilon_{\mathbf{k}}^{(0)} \tau^z - \Delta_{\sigma} \tau^x$$

being  $\tau^{\alpha}$  the Pauli matrices. Then, defining

$$\hat{s}_{\mathbf{k}\sigma}^{\alpha} \equiv \hat{\Psi}_{\mathbf{k}\sigma}^{\dagger} \tau^{\alpha} \hat{\Psi}_{\mathbf{k}\sigma} \quad \text{and} \quad \mathbf{b}_{\mathbf{k}\sigma} \equiv \begin{bmatrix} -\Delta_{\sigma} \\ 0 \\ \epsilon_{\mathbf{k}}^{(0)} \end{bmatrix}$$

one gets:

$$\hat{H} = \sum_{\mathbf{k} \in \text{MBZ}} \sum_{\sigma} \mathbf{b}_{\mathbf{k}\sigma} \cdot \hat{\mathbf{s}}_{\mathbf{k}\sigma} \quad \text{where} \quad \hat{\mathbf{s}}_{\mathbf{k}\sigma} = \begin{bmatrix} \hat{s}_{\mathbf{k}\sigma}^x \\ \hat{s}_{\mathbf{k}\sigma}^y \\ \hat{s}_{\mathbf{k}\sigma}^z \end{bmatrix} \quad (4.5)$$

The hamiltonian represents a system of spins subject to local magnetic fields, each tilted by an angle  $\tan(2\theta_{\mathbf{k}\sigma}) = \Delta_{\sigma}/\epsilon_{\mathbf{k}}^{(0)}$ , as sketched in Fig. 4.3. At any finite temperature, the ground-state of

such a system is well-known. Diagonalization of each  $h_{\mathbf{k}\sigma}$  is obtained trivially by a simple rotation around the  $y$  axis:

$$d_{\mathbf{k}\sigma} = W_{\mathbf{k}\sigma} h_{\mathbf{k}\sigma} W_{\mathbf{k}\sigma}^\dagger$$

where

$$d_{\mathbf{k}\sigma} = \begin{bmatrix} -E_{\mathbf{k}} & \\ & E_{\mathbf{k}} \end{bmatrix} \quad \text{and} \quad W_{\mathbf{k}\sigma} = \exp \left\{ i \frac{2\theta_{\mathbf{k}\sigma} - \pi}{2} \tau^y \right\}$$

Note that rotation is taken to be of an angle  $2\theta_{\mathbf{k}\sigma} - \pi$  in order to anti-align the pseudo-spin with the magnetic field of Fig. 4.3 and thus order the eigenvalues as in  $d_{\mathbf{k}\sigma}$ , with the smaller one in the top-left corner of the matrix and the larger one in the bottom-right corner. The explicit form of the transformation matrix is thus

$$W_{\mathbf{k}\sigma} = \begin{bmatrix} \cos \theta_{\mathbf{k}\sigma} & -\sin \theta_{\mathbf{k}\sigma} \\ \sin \theta_{\mathbf{k}\sigma} & \cos \theta_{\mathbf{k}\sigma} \end{bmatrix} \begin{bmatrix} & -1 \\ 1 & \end{bmatrix} = \begin{bmatrix} -\sin \theta_{\mathbf{k}\sigma} & -\cos \theta_{\mathbf{k}\sigma} \\ \cos \theta_{\mathbf{k}\sigma} & -\sin \theta_{\mathbf{k}\sigma} \end{bmatrix} \quad (4.6)$$

Eigenvalues are:

$$E_{\mathbf{k}} \equiv \sqrt{\epsilon_{\mathbf{k}}^2 + |\Delta_{\sigma}|^2}$$

(superscript “(0)” has been dropped momentarily). Notice that the presence of an absolute value makes the eigenvalues independent of the  $\sigma$  index. Eigenvector fermion operators are obtained simply as:

$$\hat{\Gamma}_{\mathbf{k}\sigma} = W_{\mathbf{k}\sigma} \hat{\Psi}_{\mathbf{k}\sigma} \quad (4.7)$$

The  $\hat{\Gamma}$  spinor operators are effectively free fermionic spinor fields and as such must be treated. Note that:

$$\begin{aligned} N &= \sum_{\mathbf{k}\sigma} \langle \hat{n}_{\mathbf{k}\sigma} \rangle \\ &= \sum_{\sigma} \sum_{\mathbf{k} \in \text{MBZ}} \langle \hat{n}_{\mathbf{k}\sigma} + \hat{n}_{\mathbf{k}+\pi\sigma} \rangle \\ &= \sum_{\sigma} \sum_{\mathbf{k} \in \text{MBZ}} \langle \hat{\Gamma}_{\mathbf{k}\sigma}^\dagger \hat{\Gamma}_{\mathbf{k}\sigma} \rangle \\ &= 2 \sum_{\mathbf{k} \in \text{MBZ}} [f(-E_{\mathbf{k}}; \beta, \mu) + f(E_{\mathbf{k}}; \beta, \mu)] \end{aligned} \quad (4.8)$$

being  $f$  be the Fermi-Dirac distribution at inverse temperature  $\beta$  and chemical potential  $\mu$ ,

$$f(\epsilon; \beta, \mu) = \frac{1}{e^{\beta(\epsilon - \mu)} + 1}$$

The 2 prefactor appeared because of spin degeneracy. Since the gapped bands refer to the smaller MBZ, thus exhibit the periodicity

$$E_{\mathbf{k}} = E_{\mathbf{k}+\pi}$$

it holds equivalently

$$N = \sum_{\mathbf{k} \in \text{BZ}} [f(-E_{\mathbf{k}}; \beta, \mu) + f(E_{\mathbf{k}}; \beta, \mu)] \quad (4.9)$$

as is obvious. The 2 prefactor was absorbed in doubling the integration region,  $\text{MBZ} \rightarrow \text{BZ}$ . Next sections are devoted to simplify the above theoretical results in order to obtain an algorithmic estimation for the magnetization  $m$ , which is just the AF instability order parameter.

### 4.2.1 Theoretical mean-field solution

A convergence algorithm can be designed to find the Hartree-Fock solution to the model. Ultimately, we aim to extract  $m$  self-consistently. Since

$$\begin{aligned} m &= \frac{1}{2L^2} \sum_{\mathbf{r}} (-1)^{x+y} \langle \hat{n}_{\mathbf{r}\uparrow} - \hat{n}_{\mathbf{r}\downarrow} \rangle \\ &= \frac{1}{2L^2} \sum_{\mathbf{k} \in \text{BZ}} \langle \hat{c}_{\mathbf{k}\uparrow}^\dagger \hat{c}_{\mathbf{k}+\boldsymbol{\pi}\uparrow} - \hat{c}_{\mathbf{k}\downarrow}^\dagger \hat{c}_{\mathbf{k}+\boldsymbol{\pi}\downarrow} \rangle \\ &= \frac{1}{2L^2} \sum_{\mathbf{k} \in \text{MBZ}} \langle (\hat{c}_{\mathbf{k}\uparrow}^\dagger \hat{c}_{\mathbf{k}+\boldsymbol{\pi}\uparrow} + \hat{c}_{\mathbf{k}+\boldsymbol{\pi}\uparrow}^\dagger \hat{c}_{\mathbf{k}\uparrow}) - (\hat{c}_{\mathbf{k}\downarrow}^\dagger \hat{c}_{\mathbf{k}+\boldsymbol{\pi}\downarrow} + \hat{c}_{\mathbf{k}+\boldsymbol{\pi}\downarrow}^\dagger \hat{c}_{\mathbf{k}\downarrow}) \rangle \end{aligned}$$

In the last passage, Eq. (4.3) has been used. Then magnetization can be computed simply as

$$m = \frac{1}{2L^2} \sum_{\mathbf{k} \in \text{MBZ}} \left[ \langle \hat{\Psi}_{\mathbf{k}\uparrow}^\dagger \tau^x \hat{\Psi}_{\mathbf{k}\uparrow} \rangle - \langle \hat{\Psi}_{\mathbf{k}\downarrow}^\dagger \tau^x \hat{\Psi}_{\mathbf{k}\downarrow} \rangle \right] \quad (4.10)$$

In this equation, spin expectation values appear:

$$\langle \hat{\Psi}_{\mathbf{k}\sigma}^\dagger \tau^x \hat{\Psi}_{\mathbf{k}\sigma} \rangle = \langle \hat{s}_{\mathbf{k}\sigma}^x \rangle$$

Now discussion is divided in two parts: zero temperature and finite temperature.

#### Zero temperature solution

For a spin system at zero temperature, the spin operator expectation value anti-aligns with the external field,

$$\langle \hat{s}_{\mathbf{k}\sigma}^x \rangle = \sin(2\theta_{\mathbf{k}\sigma})$$

(see Fig. 4.3). Now, since  $\Delta_\downarrow = -\Delta_\uparrow$ , it follows

$$\theta_{\mathbf{k}\uparrow} = -\theta_{\mathbf{k}\downarrow} \equiv \theta_{\mathbf{k}}$$

Then, from Eq. (4.10)

$$\begin{aligned} m &= \frac{1}{L^2} \sum_{\mathbf{k} \in \text{MBZ}} \sin(2\theta_{\mathbf{k}}) \\ &= \frac{1}{2L^2} \sum_{\mathbf{k} \in \text{BZ}} \sin(2\theta_{\mathbf{k}}) \end{aligned}$$

The last passage is due to the fact that the sum over the MBZ can be performed identically over  $\text{BZ} \setminus \text{MBZ}$  and yield the same result. This is because of the lattice periodicity in reciprocal space. Then, finally:

$$m = \frac{1}{L^2} \sum_{\mathbf{k} \in \text{BZ}} [W_{\mathbf{k}\uparrow}]_{11} [W_{\mathbf{k}\uparrow}^\dagger]_{21} \quad (4.11)$$

where  $\sin(2\theta_{\mathbf{k}}) = 2 \sin \theta_{\mathbf{k}} \cos \theta_{\mathbf{k}}$  has been used. As will become clear in next section, the sudden appearance of matrix elements of  $W$  is not casual.

#### Finite temperature solution

At finite temperature  $\beta$ , discussion is analogous to the section above. Here will be treated somewhat more theoretically. Define the generic order parameter:

$$\Delta_{ij}(\mathbf{k}\sigma) \equiv \langle [\hat{\Psi}_{\mathbf{k}\sigma}^\dagger]_i [\hat{\Psi}_{\mathbf{k}\sigma}]_j \rangle$$

In last section, the relevant indices  $(i, j)$  were  $(1, 2)$  and  $(2, 1)$ . Transform this order parameter,

$$\begin{aligned}
\Delta_{ij}(\mathbf{k}\sigma) &= \sum_{i'j'} \left\langle [\hat{\Gamma}_{\mathbf{k}\sigma}^\dagger]_{i'} [W_{\mathbf{k}\sigma}]_{ii'} [W_{\mathbf{k}\sigma}^\dagger]_{jj'} [\hat{\Gamma}_{\mathbf{k}\sigma}]_{j'} \right\rangle \\
&= \sum_{i'j'} [W_{\mathbf{k}\sigma}]_{ii'} [W_{\mathbf{k}\sigma}^\dagger]_{jj'} \left\langle [\hat{\Gamma}_{\mathbf{k}\sigma}^\dagger]_{i'} [\hat{\Gamma}_{\mathbf{k}\sigma}]_{j'} \right\rangle \\
&= \sum_{i'j'} [W_{\mathbf{k}\sigma}]_{ii'} [W_{\mathbf{k}\sigma}^\dagger]_{jj'} \delta_{i'j'} f([d_{\mathbf{k}\sigma}]_{ii'}; \beta, \mu) \\
&= \sum_{\ell=1}^2 [W_{\mathbf{k}\sigma}]_{\ell i} [W_{\mathbf{k}\sigma}^\dagger]_{j \ell} f((-1)^\ell E_{\mathbf{k}\sigma}; \beta, \mu) \\
&= [W_{\mathbf{k}\sigma}]_{1i} [W_{\mathbf{k}\sigma}^\dagger]_{j1} f(-E_{\mathbf{k}}; \beta, \mu) + [W_{\mathbf{k}\sigma}]_{2i} [W_{\mathbf{k}\sigma}^\dagger]_{j2} f(E_{\mathbf{k}}; \beta, \mu) \tag{4.12}
\end{aligned}$$

In the second passage this distribution appeared because an expectation value over a gas of free  $\Phi$  fermions was taken. Such an expectation value admits no off-diagonal values, hence the  $\delta_{i'j'}$ . The diagonal entries are precisely the definition of the Fermi-Dirac distribution for the given energy. At zero temperature and half-filling, the lower band  $-E_{\mathbf{k}}$  is completely filled while the upper band  $E_{\mathbf{k}}$  is empty. Substituting  $f = 1$  in the first term of line (4.12),  $f = 0$  in the second and summing  $\Delta_{12}$  and  $\Delta_{21}$  as done in Eq. (4.10), it's easy to derive the result of Eq. (4.11). At finite temperature, following the lead of the above paragraph, the antiferromagnetic instability order parameter  $m$  will be given simply by

$$m = \frac{1}{2L^2} \sum_{\mathbf{k} \in \text{BZ}} \sum_{\ell=1}^2 [W_{\mathbf{k}\uparrow}]_{\ell 1} [W_{\mathbf{k}\uparrow}^\dagger]_{2\ell} f((-1)^\ell E_{\mathbf{k}}; \beta, \mu) \tag{4.13}$$

Then: mean-field approximations yield an estimate for the magnetization at a given temperature and chemical potential just by carefully combining the elements of the diagonalizing matrix  $W$  of each Bogoliubov matrix  $h_{\mathbf{k}\sigma}$ .

#### 4.2.2 Hartree-Fock algorithm in reciprocal space

The above sections offers a self-consistency equation for the magnetization  $m$ ;  $W$  is determined by  $m$  indeed. Then a self-consistent algorithm to search for a self consistent estimate for  $m$  may be sketched:

0. Algorithm setup: initialize a counter  $i = 1$  and choose:

- the local repulsion  $U/t$  or equivalently the hopping amplitude  $t/U$ ;
- the coarse-graining of the BZ, which is, fix  $L_x$  and  $L_y$ . Then

$$k_x = 2\pi n_x / L_x \quad k_y = 2\pi n_y / L_y$$

where  $-L_j/2 \leq n_j \leq L_j/2$ ,  $n_j \in \mathbb{Z}$ ;

- the density  $n$  or equivalently the doping  $\delta \equiv n - 0.5$ ;
- the inverse temperature  $\beta$ ;
- the number of iterations  $p \in \mathbb{N}$ ;
- the mixing parameter  $g \in [0, 1]$ ;
- the tolerance parameters  $\Delta_m, \Delta_n \in \mathbb{R}$  (respectively for magnetization and density);

1. Select a random starting value  $m_0 \in [0, 1]$ ;
2. For each slot of the BZ, initialize the appropriate  $2 \times 2$  matrix  $h_{\mathbf{k}\uparrow}$  as in Eq. (4.4);
3. For the given hamiltonian, find the optimal chemical potential  $\mu$  as follows:

- a) Diagonalize  $h_{\mathbf{k}\uparrow}[m_0, U]$  and obtain its eigenvalues  $\pm E_{\mathbf{k}}[m_0, U]$ ;

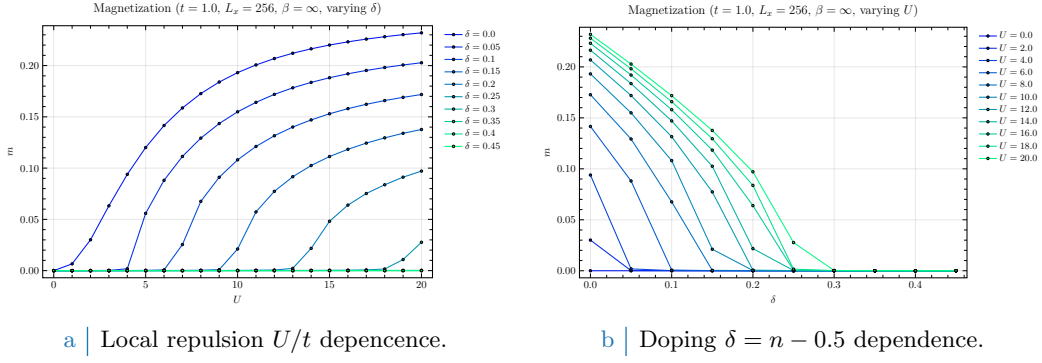


**Figure 4.4** | Plots of the zero-temperature AF instability order parameter  $m$  as a function of both the local repulsion  $U/t$  (Fig. 4.4a) and the doping  $\delta = n - 1/2$  (Fig. 4.4b).

b) Define the function of the chemical potential  $\mu$ ,

$$\delta n(\mu; \beta, m_0, U) \equiv 2 [f(-E_{\mathbf{k}}[U, m_0]; \beta, \mu) + f(E_{\mathbf{k}}[U, m_0]; \beta, \mu)] - n$$

c) Find the root of  $\delta n$ ,

$$\delta n(\mu_0) = 0$$

Then  $\mu_0$  is the chemical potential which, at magnetization  $m_0$ , realizes the best approximation of density  $n$ ;

4. Diagonalize the matrix  $h_{\mathbf{k}\uparrow}$  and obtain  $d_{\mathbf{k}\uparrow}$ ;
5. Compute  $m$  using Eq. (4.13) with chemical potential  $\mu_0$  and update the counter,  $i \rightarrow i + 1$ ;
6. Check if  $|m - m_0| \leq \delta_m$ :
  - If yes, halt;
  - If not: check if  $i > p$ 
    - If yes, halt and consider choosing better tolerance and model parameters;
    - If not, define

$$m_0 = gm + (1 - g)m_0$$

(logical assignment notation used) and repeat from step 2.

In next section some results are briefly shown.

## Results

The algorithm sketched in the above paragraph was ran with the following setup:

```

1 UU = [U for U in 0.5:0.5:20.0]      # Local repulsions
2 LL = [256]                          # Lattice sizes
3 dd = [d for d in 0.0:0.05:0.45]    # Dopings
4 bb = [100.0, Inf]                  # Inverse temperatures
5 p = 100                             # Max number of iterations
6 dm = 1e-4                          # Tolerance on magnetization
7 dn = 1e-2                          # Tolerance on density
8 g = 0.5                            # Mixing parameter

```

In Fig. 4.4 plots at  $\beta = \infty$  of the magnetization  $m$  is reported. As is evident in Fig. 4.4a, disrupts AF ordering; the horizontal asymptote lowers as  $\delta$  gets bigger, a mere consequence of the fact that the free space at each single-particle state in  $k$ -space shrinks as density increases; also, for  $\delta > 0$ , a finite magnetization  $m$  exists only for  $U \geq U_c[\delta]$  (a critical value parametrically dependent

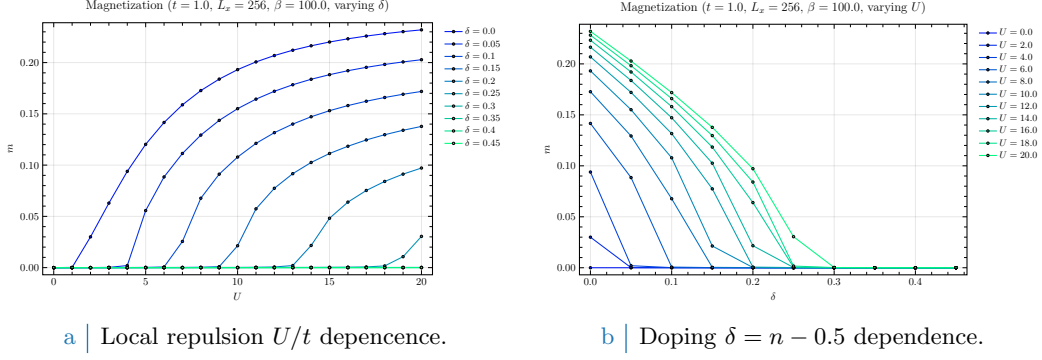


**Figure 4.5** | Plots of the zero-temperature AF instability order parameter  $m$  as a function of both the local repulsion  $U/t$  (Fig. 4.5a) and the doping  $\delta = n - 1/2$  (Fig. 4.5b).

on doping). Fig. 4.4b shows the dependence of magnetization on doping at various fixed local repulsions  $U$ : once again, to dope the material disrupt AF ordering. Identical analysis have been performed for finite temperatures, leading to analogous results as long as  $\beta \gtrsim 10$  and to  $m \simeq 0$  for higher temperatures (predictably). For the sake of completeness, results are plotted in Fig. 4.5: the only relevant difference with Fig. 4.4 is that for null doping and null local-interaction  $U$ , as is intuitive, the self-consistent magnetization is null. This result, with respect to the one of Fig. 4.4a, is more physical.

#### 4.2.3 An alternative (less efficient) real-space approach

The theoretical derivation of the above paragraphs offers a simple description of the system anti-ferromagnetic instability as the instauration of a ground-state of quasiparticles. Here a self-consistent algorithmic extraction of the expected magnetization is presented, following [7]. Note that this algorithm is by far the least efficient, being performed in real space with dimensional exponential scaling in terms of computational time. It is here presented just for completeness as an alternative derivation. This algorithm can become useful for simulations not preserving space-translational invariance, e.g. introducing some degree of disorder. Consider a square lattice of  $L_x \times L_y$  sites: the hamiltonian will be a matrix of dimension  $2L_x L_y \times 2L_x L_y$ ,

$$[\hat{H}]_{(\mathbf{r}\sigma)(\mathbf{r}'\sigma')} = \langle \Omega | \hat{c}_{\mathbf{r}\sigma} \hat{H} \hat{c}_{\mathbf{r}'\sigma'}^\dagger | \Omega \rangle$$

For simplicity, in the following  $D \equiv 2L_x L_y$ . In this context, the following convention is used: the rows/column index entry  $\alpha = (\mathbf{r}\sigma)$  is associated to a specific site  $\mathbf{r} = (x, y)$  and spin  $\sigma$  through the relation

$$\alpha = 2j_{\mathbf{r}} - \delta_{\sigma=\uparrow} \quad \text{where} \quad j_{\mathbf{r}} = x + (y-1)L_x$$

Let me break this through. For each site  $\mathbf{r}$ , two sequential indices are provided ( $2j_{\mathbf{r}} - 1$ , hosting spin  $\uparrow$ , and  $2j_{\mathbf{r}}$ , hosting spin  $\downarrow$ ).  $j_{\mathbf{r}}$  just orders the site rows-wise. This way,  $(x, 1)$  is assigned to  $j_{(x,1)} = x$ , while its NN one site above  $(x, 2)$  is assigned to an entry shifted by  $L_x$ ,  $j_{(x,2)} = x + L_x$ . This is just a way of counting the site of a finite square lattice by sweeping along a row and then moving to the row above. Fig. 4.6 reports a scheme of the used site ordering.

Within this convention, matrix elements  $H_{\alpha\beta}$  are defined by:

- If  $\sigma = \sigma'$  and  $\mathbf{r}, \mathbf{r}'$  are NN, the matrix entry is  $-t$ . In terms of the used greek indices,  $\alpha$  and  $\beta$  satisfy said requirement if  $|\alpha - \beta| = 2$  (horizontal hopping) or  $|\alpha - \beta| = 2L_x$  (vertical hopping). Along column  $\alpha$  of the hamiltonian matrix, the elements  $-t$  appear at positions

$$(\alpha \pm 2L_x) \bmod D \quad \text{and} \quad (\alpha \pm 2) \bmod D$$

- If  $\mathbf{r} = \mathbf{r}'$  and  $\sigma = \sigma'$  (along the diagonal), the local interaction with the mean field is given by the matrix element

$$-mU \times (-1)^{x+y} \times (-1)^{\delta_{\sigma=\downarrow}}$$

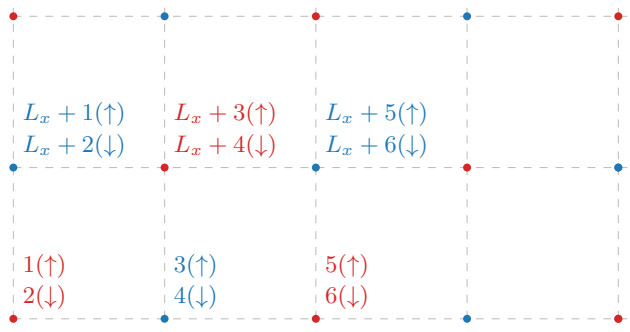


Figure 4.6 | Schematics of the site ordering on a square lattice performed by sweeping along rows. Left-bottom side is one corner of the lattice. Red sites are characterized by  $x+y$  being odd, blue sites by being even. The number reported near to each site is the  $\alpha$  entry in the matrix representation for a finite square lattice.

Starting from a given entry  $\alpha$ ,  $j_{\mathbf{r}}$  is retrieved simply by  $j_{\mathbf{r}} = \lfloor \alpha/2 \rfloor$ , and then

$$x + y = (j_{\mathbf{r}} + 1) - \left\lfloor \frac{j_{\mathbf{r}}}{L_x} \right\rfloor (L_x - 1)$$

Then the  $j_{\mathbf{r}}$ -th  $2 \times 2$  block along the diagonal will be given by

$$(-1)^{x+y} \underbrace{\begin{bmatrix} -mU & \\ & mU \end{bmatrix}}_{\mathcal{B}}$$

Note that the resulting block diagonal contribution to the hamiltonian is shaped like follows (assume  $L_x$  to be even):

$$\begin{array}{c} \begin{matrix} 1 & 2 & \cdots & L_x - 1 & L_x & L_x + 1 & L_x + 2 & \cdots \end{matrix} \\ \begin{matrix} 1 \\ 2 \\ \vdots \\ L_x - 1 \\ L_x \\ L_x + 1 \\ L_x + 2 \\ \vdots \end{matrix} \end{array} \left[ \begin{array}{cccccccc} \mathcal{B} & & & & & & & \\ & -\mathcal{B} & & & & & & \\ & & \ddots & & & & & \\ & & & \mathcal{B} & & & & \\ & & & & -\mathcal{B} & & & \\ & & & & & -\mathcal{B} & & \\ & & & & & & \mathcal{B} & \\ & & & & & & & \ddots \end{array} \right]$$

Along the same row, on the diagonal the  $2 \times 2$  blocks  $\mathcal{B}$  alternate signs; changing row (in the example above, at positions  $L_x, L_x + 1$ ), due to the anti-ferromagnetic configuration of local mean-fields, an additional  $-1$  is included. If  $L_x$  is taken to be odd, the diagonal blocks just alternate signs all the way.

These prescriptions allow to build from scratch the hamiltonian matrix. After that, diagonalization provides  $D$  orthonormal eigenvectors  $\mathbf{v}^\ell \in \mathbb{C}^{D \times D}$  with  $\ell = 1, \dots, D$ , each associated to a precise eigenvalue  $\epsilon^\ell \in \mathbb{R}$ . At equilibrium, electrons will fill up the energy eigenstates according to,

$$\langle \hat{n}_{\mathbf{r}\sigma} \rangle = \sum_{\ell=1}^D |v_\alpha^\ell|^2 f(\epsilon^\ell; \beta, \mu) \quad \text{where} \quad \alpha = (\mathbf{r}\sigma)$$



For a fixed filling  $n = N/D$ , the chemical potential must satisfy

$$\begin{aligned}
n &= \frac{1}{D} \sum_{\mathbf{r}\sigma} \langle \hat{n}_{\mathbf{r}\sigma} \rangle \\
&= \frac{1}{D} \sum_{\mathbf{r}\sigma} \sum_{\ell=1}^D |v_{\alpha}^{\ell}|^2 f(\epsilon^{\ell}; \beta, \mu) \\
&= \frac{1}{D} \sum_{\ell=1}^D f(\epsilon^{\ell}; \beta, \mu)
\end{aligned}$$

since the  $\mathbf{v}^{\ell}$  eigenvectors are orthonormal. The chemical potential for the half-filled model is already known to be

$$\mu|_{n=1/2} = -\frac{U}{2}$$

as evident from Eq. (4.2). Average magnetization is then given by

$$\begin{aligned}
m &= \frac{1}{D} \sum_{\mathbf{r}} (-1)^{x+y} [\langle \hat{n}_{\mathbf{r}\uparrow} \rangle - \langle \hat{n}_{\mathbf{r}\downarrow} \rangle] \\
&= \frac{1}{D} \sum_{\lambda=1}^{D/2} (-1)^{(\lambda+1) - \lfloor \lambda/L_x \rfloor (L_x-1)} \sum_{\ell=1}^D \left[ |v_{2\lambda-1}^{\ell}|^2 - |v_{2\lambda}^{\ell}|^2 \right] f(\epsilon^{\ell}; \beta, \mu)
\end{aligned} \tag{4.14}$$

since  $\mathbf{r} \uparrow$  is associated to an odd index entry, while  $\mathbf{r} \downarrow$  to the following even entry. The associated HF algorithm is identical to the one presented in Sec. 4.2.2, with the following substitutions:

2. Initialize the hamiltonian matrix  $H_{\alpha\beta}$  matrix according to the initialized  $m_0$  and the site indexing rules of Fig. 4.6;
4. Diagonalize the matrix associated to the operator  $\hat{H}_{\alpha\beta} - \mu \hat{N}$  collecting the  $\mathbf{v}^{\ell}$  eigenvectors;
5. Compute  $m$  using Eq. (4.14) and update the counter,  $i \rightarrow i + 1$ ;



# Bibliography

- [1] Zhangkai Cao et al. *p-wave superconductivity induced by nearest-neighbor attraction in the square-lattice extended Hubbard model*. en. arXiv:2408.01113 [cond-mat]. Jan. 2025. DOI: [10.48550/arXiv.2408.01113](https://doi.org/10.48550/arXiv.2408.01113). URL: <http://arxiv.org/abs/2408.01113> (visited on 03/15/2025).
- [2] Piers Coleman. *Introduction to Many-Body Physics*. Cambridge University Press, 2015.
- [3] Michele Fabrizio. *A Course in Quantum Many-Body Theory*. Springer, 2022.
- [4] Gabriele Giuliani and Giovanni Vignale. *Quantum Theory of the Electron Liquid*. Cambridge University Press, 2005.
- [5] Giuseppe Grosso and Giuseppe Pastori Parravicini. *Solid State Physics*. Second Edition. Academic Press, 2014.
- [6] J. E. Hirsch. “Two-dimensional Hubbard model: Numerical simulation study”. In: *Phys. Rev. B* 31 (7 Apr. 1985), pp. 4403–4419. DOI: [10.1103/PhysRevB.31.4403](https://doi.org/10.1103/PhysRevB.31.4403). URL: <https://link.aps.org/doi/10.1103/PhysRevB.31.4403>.
- [7] Robin Scholle et al. “Comprehensive mean-field analysis of magnetic and charge orders in the two-dimensional Hubbard model”. In: *Phys. Rev. B* 108 (3 July 2023), p. 035139. DOI: [10.1103/PhysRevB.108.035139](https://doi.org/10.1103/PhysRevB.108.035139). URL: <https://link.aps.org/doi/10.1103/PhysRevB.108.035139>.